5-2016

# Influence of Hydrogen Concentration and Distribution on Fracture in Nickel

Arturo Sucre Melfi
*University of Arkansas, Fayetteville*

# Influence of Hydrogen Concentration and Distribution on Fracture in Nickel

Arturo Sucre Melfi

University of Arkansas, Fayetteville
May 2016

**Acknowledgements**

First, I would like to thank the University of Arkansas Honors College. This research was supported by an Honors College Undergraduate Research Grant. I also would like to mention my financial sponsor who made it possible for me to do my undergraduate studies in mechanical engineering at the University of Arkansas, SENACYT-IFHARU from Panama. Most important, I would like to recognize and thank my research advisor, Dr. Douglas Spearot, for his guidance and mentoring throughout the research and thesis preparation processes. From helping me learn LAMMPS, to help me understand and analyze the obtained results. I would like to also thank the Arkansas High Performance Computing Center (AHPCC), for allowing me to use their facilities to perform my simulations. Finally, I appreciate the help from the Department of Mechanical Engineering at the University of Arkansas, for letting me work in my research at the NANO building and at the MEEG building computer labs.

**Table of Contents**

## Introduction

Material failure is one of the most important problems in materials science and engineering. Depending on the type of material, there exists different types of failure. Ductile materials, before fracturing, suffer first a yielding failure which causes plastic deformation. This means that the material will deform before a total fracture occurs. On the other hand, less ductile, or brittle, materials such as ceramics, fracture without any manifestation of plastic deformation due to the growth and coalescence of small cracks on the atomic level. One way of knowing if a material is either ductile or brittle is to subject it to a tensile test and analyzing the resulting stress versus strain graph. An example showing the curves for both types of materials is shown in Figure 1.

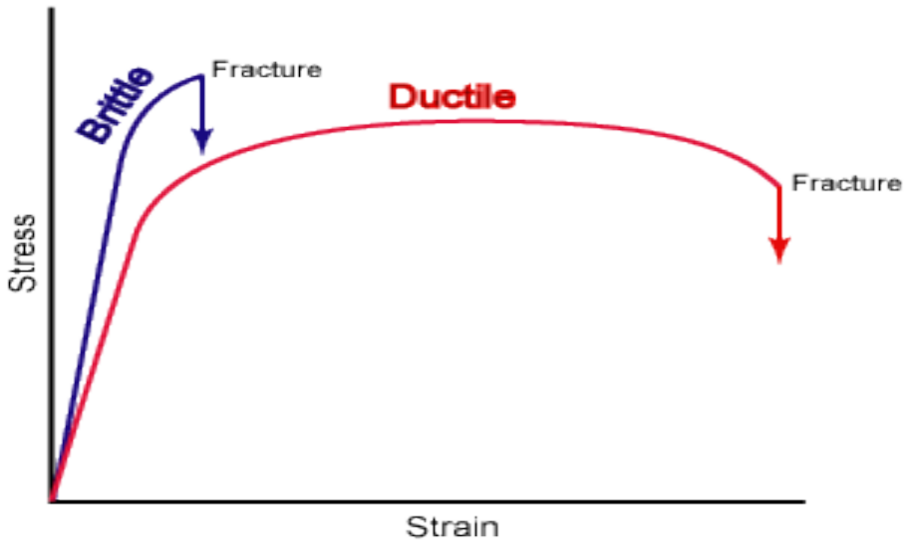


*Figure 1. Stress-strain curves for brittle and ductile materials. [1]*

Metals, which usually fall in the ductile material category, may suffer from embrittlement, which is a loss of ductility of the material, thus failing without the expected amount of ductility. Causes of embrittlement include: environmentally induced cracking, stress cracking due to

corrosion, corrosion fatigue, liquid metal embrittlement and hydrogen embrittlement [2]. Hydrogen embrittlement, also called hydrogen induced cracking (HIC) or hydrogen attack, causes a material to become brittle due to the presence of hydrogen at interstitial lattice sites. This phenomenon was first noted in 1875 by W. H. Johnson. In his work, "On Some Remarkable Changes Produced in Iron by the Action of Hydrogen and Acids", he observed that the piece of iron he was studying was suffering from a decrease of toughness due to the presence of hydrogen [3].

There is no exact theory that explains how hydrogen diffuses into metals and then how hydrogen changes the atomic behavior leading to brittle failure. However, there are three proposed and generally accepted factors that may cause a metal to suffer from hydrogen embrittlement: Mechanical (stresses, cyclical loading, manufacturing processes), Environmental (temperature, concentration of hydrogen) and Material (crystal structure, phase composition) [4], as shown in Figure 2.

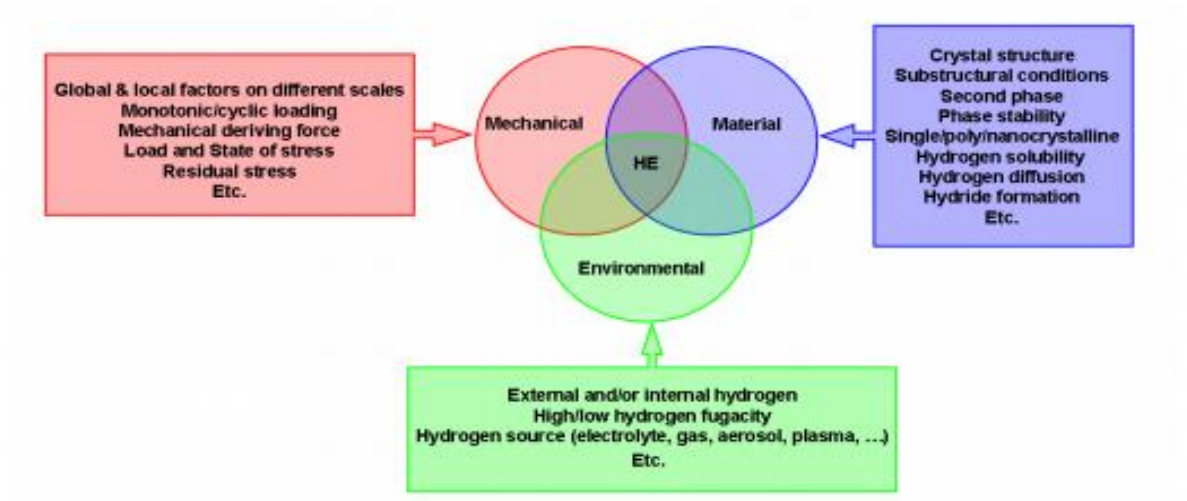


*Figure 2. Hydrogen Embrittlement Factors. [4]*

As stated above, when metals are subjected to stresses higher than their yield strength, they experience plastic deformation. Then, once the stress is elevated beyond the ultimate strength of the material, cracks on the mircro and nano scale will begin to emerge. The reason why metals typically don't fracture at the yield strength is dislocations. Dislocations are crystallographic defects within the crystal structure of a metal, which aid the relief of the metal from stress. Dislocations move around within the crystal structure "carrying" the plastic deformation. When hydrogen is absorbed at the surface, it causes surface embrittlement, but if it diffuses into the matrix, it may cause hydride formation and/or bulk embrittlement [5]. Several mechanisms have been proposed to explain the hydrogen embrittlement process. Some examples of these mechanisms are [6]:

- Internal Pressure Mechanism: Presence of hydrogen at defects in the crystal structure increases the internal pressure, thus lowering the apparent fracture stress.
- Surface Energy Mechanism: Adsorption of hydrogen reduces the amount of surface energy required for crack propagation.
- Hydrogen Enhanced Decohesion Mechanism (HEDE): Presence of hydrogen in the lattice reduces the cohesive strength of the interatomic bonds in the crystal structure.
- Hydrogen Enhanced Localized Plasticity Mechanism (HELP): Adsorption of hydrogen increases dislocation motion and generation.

The last two of these models are briefly explained in the following paragraphs.

The Hydrogen Enhanced Decohesion (HEDE) Mechanism states that the presence of hydrogen atoms in the lattice reduces the cohesive bonding strength between metal atoms [4].

Normally, a metal's lattice will consist of closely packed atoms with a certain level of bonding strength. But, when hydrogen atoms diffuse into the crystal structure of the metal, the strength of the bonds holding the atoms together reduces, thus making it easier for them to be broken apart during crack propagation. Not only does HEDE makes it easier for cracks to form, but it also causes cracks to grow larger and faster, reducing the ductility of the metal.

The Hydrogen Enhanced Localized Plasticity (HELP) Mechanism states that the presence of hydrogen near the crack tip causes a larger rate of dislocation generation and motion [6, 19-22]. This increase in dislocation generation might seem counterintuitive to what hydrogen embrittlement causes. An increase of dislocation motion, or plastic flow, would mean that a material becomes even more ductile. Beachem [7] suggested that the presence of hydrogen causes dislocations to behave in such way that plastic deformations due to crack growth in the atomic level causes a brittle behavior of the metal in the macroscopic scale. Another effect caused by the HELP mechanism is that it causes a change of shape of the crack tip. Normally, crack tips are sharp, but when the HELP mechanism happens, the crack tip becomes blunt. This change in shape might cause a decrease in the crack tip velocity and an increase in dislocation generation. An illustration of the HELP mechanism is shown in Figure 3.

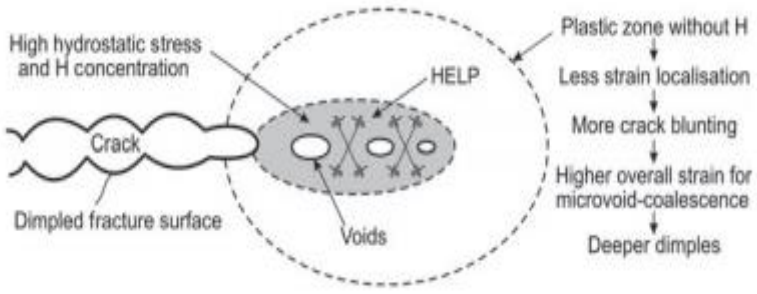


*Figure 3. HELP Mechanism schematic. [6]*

*Applications Related to Hydrogen Embrittlement*

Finding a solution to the hydrogen embrittlement problem will significantly impact many applications used in the science and engineering fields. Some examples of these applications are:

- Hydrogen Fuel Cell Vehicles (storage tanks used to hold hydrogen)
- Gas Transfer Systems
- Structural materials used in nuclear reactors
- Bridges (bolts, rods, washers)

This last application has a recent example of the damage that hydrogen embrittlement can cause. Six months before opening the East Span of the San Francisco-Oakland Bay Bridge, 32 out of 96 anchor rods failed during testing. It was determined that the primary reason of failure of these rods was environmental hydrogen embrittlement [8].

It has been clearly stated that hydrogen embrittlement presents a serious problem when working with metals. One important aspect still being studied in the hydrogen embrittlement community is how different hydrogen concentrations within the crystal structure affect the severity of the embrittlement. Accordingly, the main objective of this research is to address this specific aspect of the hydrogen embrittlement problem. The main goal is to relate the concentration and distribution of hydrogen near the crack tip in single crystal nickel to how a crack behaves. The behavior of the crack is divided in two different categories: velocity of crack tip and dislocation nucleation. In order to accurately compare how the crack behaves with and without the presence of hydrogen, two main models were built. The first model is a 3D single crystal nickel sample, while the second model is a 3D single crystal nickel sample with hydrogen atoms in different concentrations and distributed within different regions near the crack tip.

## Methods and Modelling

*Methods Software*

In order to model crack propagation, computer simulation is performed using the molecular dynamics (MD) method. Molecular dynamics calculates the time dependent behavior of a molecular system [9]. In the system built, the interactions between atoms are modeled using an interatomic potential, which is a function used to describe the interaction between atoms and their potential energy with respect to each other [10]. The software used to perform the molecular dynamics simulations is called LAMMPS (Large-scale Atomic/Molecular Massively Parallel Simulator). LAMMPS is a classical molecular dynamics simulation code [11]. LAMMPS is distributed by a U.S. Department of Energy laboratory, Sandia National Laboratories located in Albuquerque, New Mexico. In order to visualize the MD simulation results, small movies outputted from LAMMPS are imported to OVITO (Open Visualization Tool), a scientific visualization and analysis software used for atomistic simulations [12]. All simulations visualization, data acquisition and some data analysis are performed using OVITO [13].

*Facilities*

All MD simulations were performed at the Arkansas High Performance Computing Center (AHPCC). Specifically, MD simulations were conducted using the Razor II system. Razor II is an IBM iDataPlex system composed of 112 compute nodes, each with two eight-core Intel Xeon E5-2670 “Sandy Bridge” 2.6 GHz processors, for a total of 1,792 cores and a peak performance of 37.7 TFlop/s. Each node has a capacity of 32 GB of memory [14]. Visualization of the MD simulation results and all data analysis were performed on a personal laptop.

*Building the Nickel Model*

LAMMPS is used to build the 3D single crystal nickel model. The geometry of the model is created using known nickel characteristics. Nickel has a face-centered cubic unit cell and its lattice parameter, the dimension of its unit cell, is 3.52 Angstroms (Å). One angstrom is equal to $1 \times 10^{-10}$ meter. The dimensions used to create this model are the following:

- Dimension in X (Length): 100 unit cells
- Dimension in Y (Width): 80 unit cells
- Dimension in Z (Thickness): 20 unit cells

The actual size of the model is the number of unit cells multiplied by the lattice parameter. (i.e., the actual length of the model is 100 x 3.52 Å = 352 Å). The Miller indices of the lattice, defining the lattice orientation, used are the following:

- X [1 0 0]
- Y [0 1 0]
- Z [0 0 1]

In this nickel model, two nickel potentials are used [15,16], both of which are embedded atom method (EAM) potentials. The EAM is a semi-empirical interatomic potential model used to calculate the total energy of a many-atom metallic system [5].

After specifying the interatomic potentials to be used, 5 different regions within the model are created, all of them containing nickel atoms as shown in Figure 4. After an energy minimization procedure to ensure that all atoms are initially in minimum energy positions, atomic velocities are assigned according to the total system temperature of 298 K. The energy minimization algorithm works by iteratively adjusting atom coordinates [17]. In order to insert a crack in the system, the

LAMMPS “neigh_modify” command was used, separating two regions on the left hand side of the model as shown in Figure 4. To apply deformation, the atoms of the upper region were set to have a velocity of 0.3 Å/fs. Further, a gradient velocity was applied from 0.0 Å/fs at the lower boundary to 0.3 Å/fs at the upper boundary. The simulation is set to run using the NVE (constant number of atoms, constant volume, and constant total energy) ensemble for 40,000 time steps with a time step of 0.001 picoseconds per time step, which is sufficient for crack growth and dislocation nucleation. Finally, using the LAMMPS “dump” command, snapshots of the atom positions are outputted to a file, to be analyzed later using OVITO.

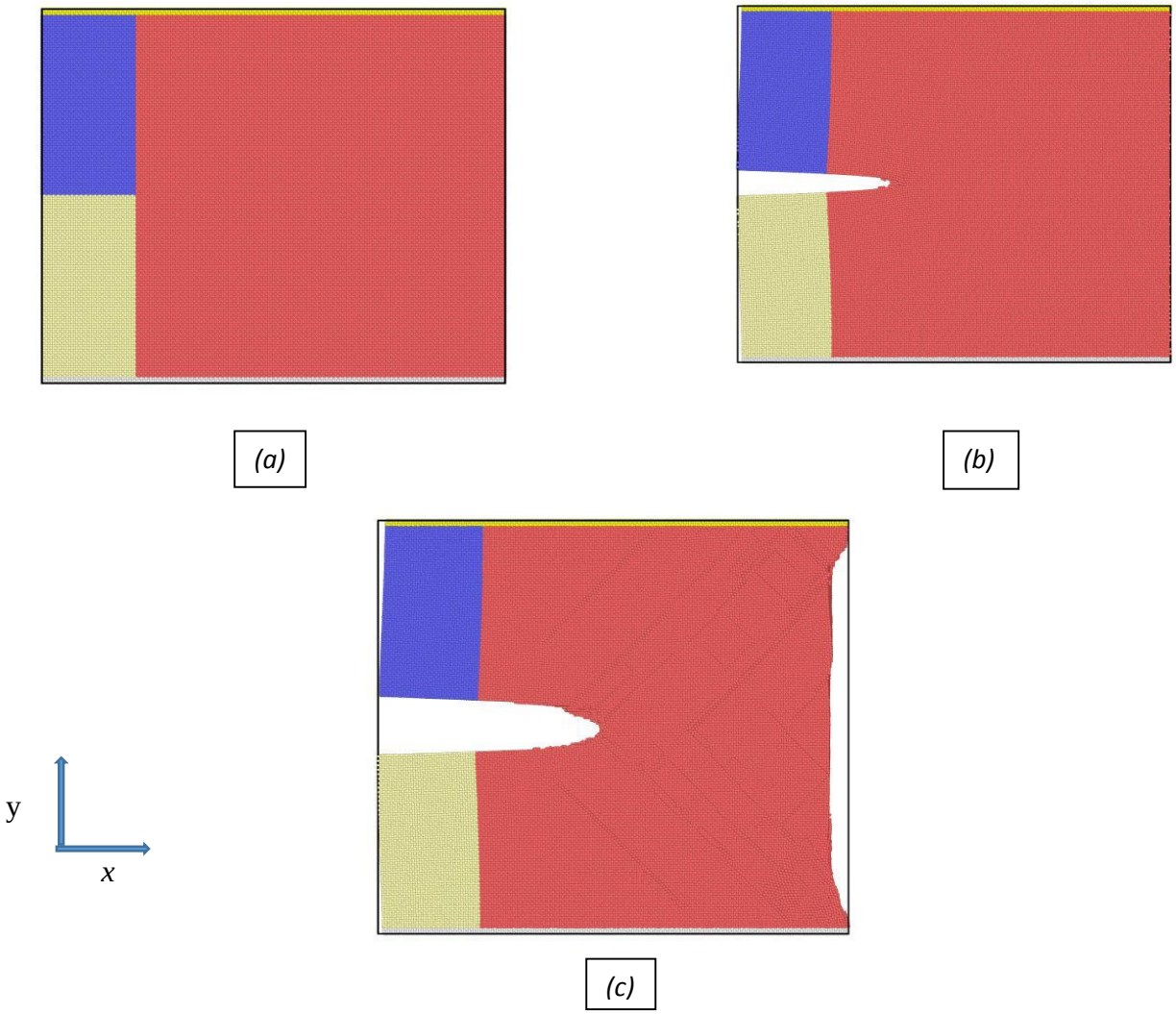


*Figure 4. (a) Crack at t=0 ps, (b) Crack at t=10 ps, (c) Crack at t=20 ps. [13]*

The next step in the research was to insert hydrogen into the single crystal nickel lattice, thus creating the second main model.

*Building the Nickel-Hydrogen Model*

In order to create the Ni-H model, hydrogen atoms were inserted into the single crystal model. The geometry and dimensions from the first model are maintained, but some additions and changes to the code were done. For these calculations, only the potential by Angelo et al. [16] can be used as it includes the Ni-H interactions. Also, besides adding hydrogen to the interatomic potential, a region where the hydrogen atoms will be inserted is created. This region is located in an area where the crack propagates. Using LAMMPS "create_atoms" command, the hydrogen atoms were added randomly to the model. This approach assumes that the hydrogen has already diffused into the nickel lattice and become trapped at the crack tip; if desired, it is possible to compute hydrogen diffusion rates through the nickel lattice using standard methods within MD. In order to avoid atoms being misplaced and the system becoming unstable, an energy minimization was performed on the system using the LAMMPS "minimize" command. The remained of the simulation procedures are identical to the pure nickel fracture model.

After making these changes and additions, it was important to take a look at the two main aspects of this research, the concentration of hydrogen and the size of the region containing hydrogen near the crack tip. The first step was to specify how many regions near the crack tip were to be studied, and it was decided that four regions were to be built. These regions will vary in their size in the X and Y directions, all of them having the same size in the Z direction as the main model. The first region is called 'Single-Single'; its name being in an X-Y direction format. The

second region is called ‘Single-Double’, meaning that it has the same size in X as the first region, but has double the size in the Y direction of it. The third region is called ‘Double-Single’ (double in X, same in Y as the first region) and finally the last region is ‘Double-Double’ (double in X and in Y than the first region). Table 1 specifies the dimensions of each region.

| Hydrogen Regions Dimensions | | | |
|---|---|---|---|
| Region Name | X (Unit Cells) | Y (Unit cells) | Z (Unit cells) |
| Single-Single | 20 | 4 | 20 |
| Single-Double | 20 | 8 | 20 |
| Double-Single | 40 | 4 | 20 |
| Double-Double | 40 | 8 | 20 |

*Table 1. Dimensions of hydrogen regions.*

The next step before starting to run the simulations, was to define the hydrogen concentration. In order to do that, it is important to know the amount of nickel atoms inside each region. Since nickel has a FCC unit cell, there are 8 corner atoms, but since each corner atom is shared by eight unit cells, there is only 1/8 of an atom in each corner of a unit cell. Likewise, there are six face atoms, and each one of those is shared by two unit cells, so there is 1/2 atom in each face of the unit cell. As shown in Equation 1, there are four atoms in total in each FCC unit cell.

$$\left(8 * \frac{1}{8}\right)_{corner\ atoms} + \left(6 * \frac{1}{2}\right)_{face\ atoms} = 4\ Ni\ atoms \quad (1)$$

In order to know the exact amount of nickel atoms in each region, the three unit cells dimensions (length, width, thickness) and the number of nickel atoms per unit cell (four) were multiplied as shown in Equation 2:

$$\#Ni\ atoms\ in\ region = L * W * t * \#Ni\ atoms\ per\ unit\ cell \quad (2)$$

After the number of nickel atoms in each region is calculated, the hydrogen concentration in atomic percent was calculated using Equation 3:

$$\#H\ atoms = \frac{\%H * \#Ni\ atoms\ in\ region}{1 - \%H} \quad (3)$$

The hydrogen concentrations (in atomic percent) chosen to study in this research are 0.1%, 0.5%, 1%, and 10%. Table 2 presents the number of hydrogen atoms introduced into each region for each of the chosen concentrations.

| # Hydrogen Atoms | | | | | | | | |
|---|---|---|---|---|---|---|---|---|
| Region | Single-Single | | Single-Double | | Double-Single | | Double-Double | |
| # Ni atoms | 6400 | | 12800 | | 12800 | | 25600 | |
| | %H | #H atoms | %H | #H atoms | %H | #H atoms | %H | #H atoms |
| | 0.1 | 6 | 0.1 | 13 | 0.1 | 13 | 0.1 | 26 |
| | 0.5 | 32 | 0.5 | 64 | 0.5 | 64 | 0.5 | 128 |
| | 1 | 64 | 1 | 128 | 1 | 128 | 1 | 256 |
| | 10 | 640 | 10 | 1280 | 10 | 1280 | 10 | 2560 |

*Table 2. Number of Hydrogen atoms for each concentration introduced in each region.*

The four known concentrations were added to each region, yielding a total number of 16 simulations to be compared with the nickel models without hydrogen. Figure 5 shows how the Ni-H model looks like using OVITO. The model used for this image was the 'Double-Double' with a 10% hydrogen concentration. Hydrogen atoms are artificially enlarged to show their position within the model.

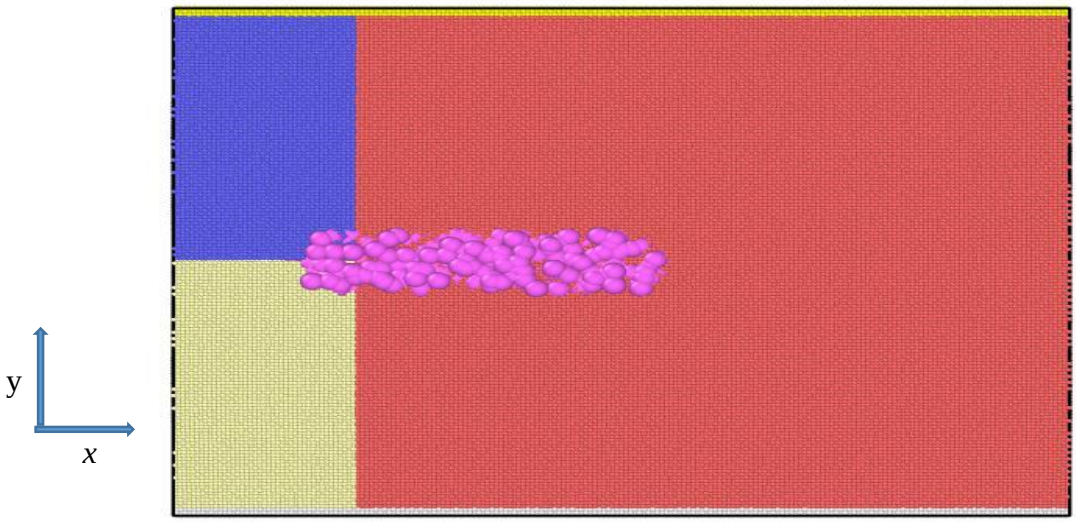


*Figure 5. Ni-H model (H atoms enlarged for viewing purposes). [13]*

One important aspect that was taken into account when analyzing the results of the simulation was the importance of the boundary conditions of each model. When analyzing the results, there was a point during each simulation where the plastic deformations caused by the crack growth reaches the fixed boundaries of the model. Taking this into account, the results and analysis where performed until the moment this phenomenon happens. Snapshots of the crack propagating alongside each model can be found in Appendix B.

**Results**

As stated above, 18 different simulations were performed, 2 3D single crystal nickel models and 16 3D single crystal nickel models with hydrogen present in different concentrations and regions. The two aspects studied and compared between these models were the crack tip velocity and the dislocation nucleation near the crack tip.

*Crack tip Velocity*

The crack tip velocity for each simulation was studied using OVITO, more specifically, the "inspect particle tool" within OVITO. The inspect particle tool provides information on any particle inside the model, such as position with respect to the X, Y and Z directions of the model. So, for each time step, a particle located at the crack tip was selected in order to know its position with respect to the length of the model. This method enabled a calculation of the "distance" that the crack tip has moved during each time step. Figure 6 shows an example of the usage of the inspect particle tool.

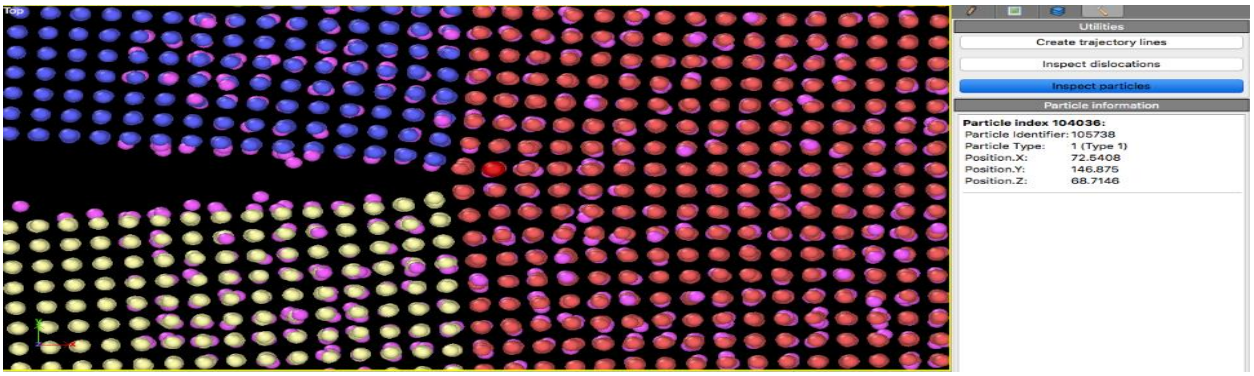


*Figure 6. Inspect particle tool used to find the distance of the crack tip. [13]*

After evaluating the crack in order to know the distance traveled by it at each time step, a 'Distance versus Time' graph was built with the known data for each region size and for each hydrogen concentration. Graphs showing the crack propagation in each of the four regions for each hydrogen concentration studied are shown in Figures 7-10. Two different nickel only models are also included in these graphs. The nickel model 1 is using the Foiles et al. [15] potential, while the nickel model 2 is using the Angelo et al. [16] potential.

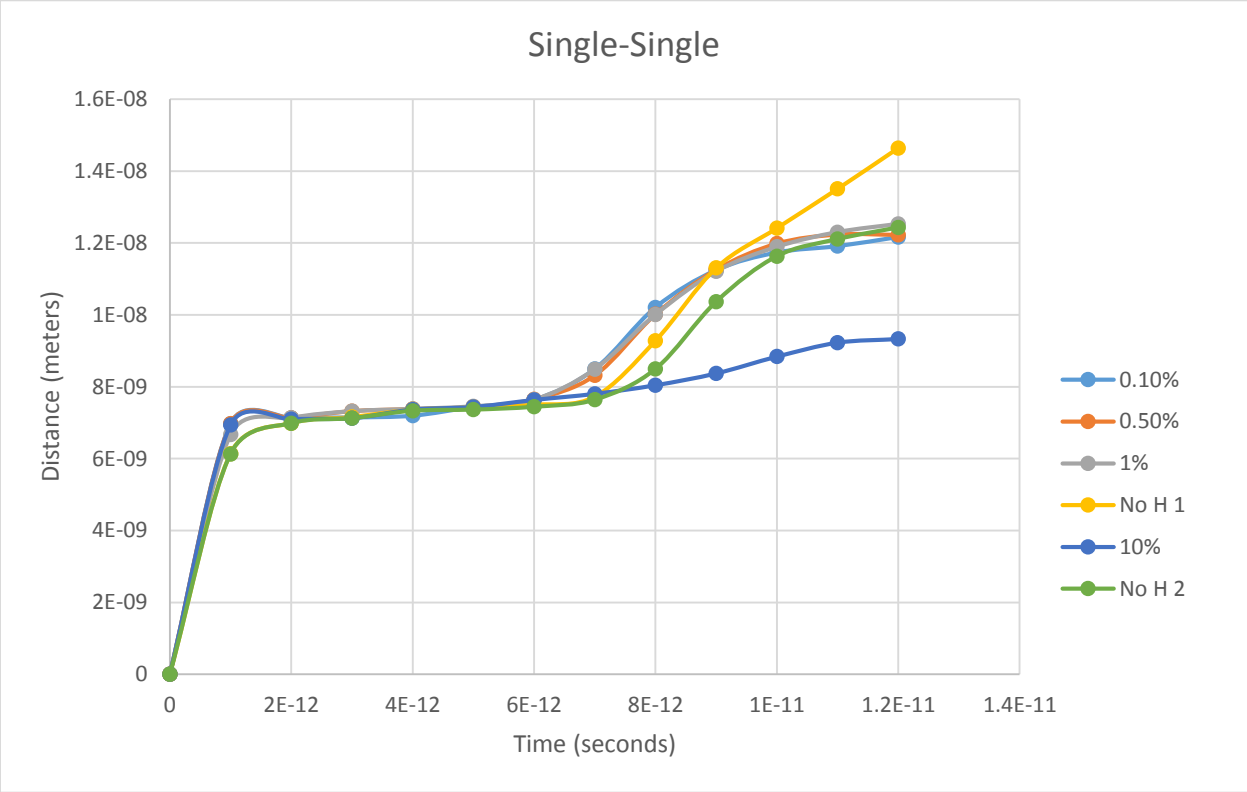


*Figure 7. 'Single-Single' D vs T graph comparing hydrogen concentrations.*

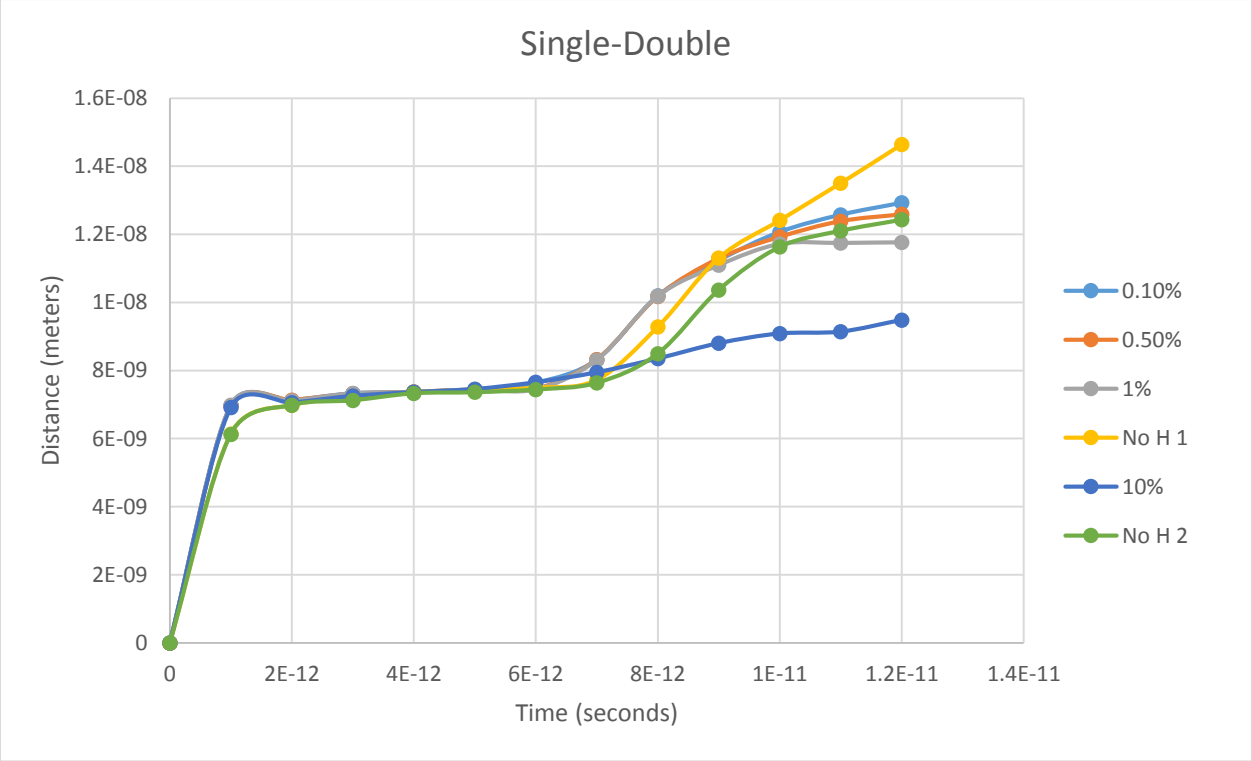


*Figure 8. 'Single-Double' D vs T graph comparing hydrogen concentrations.*

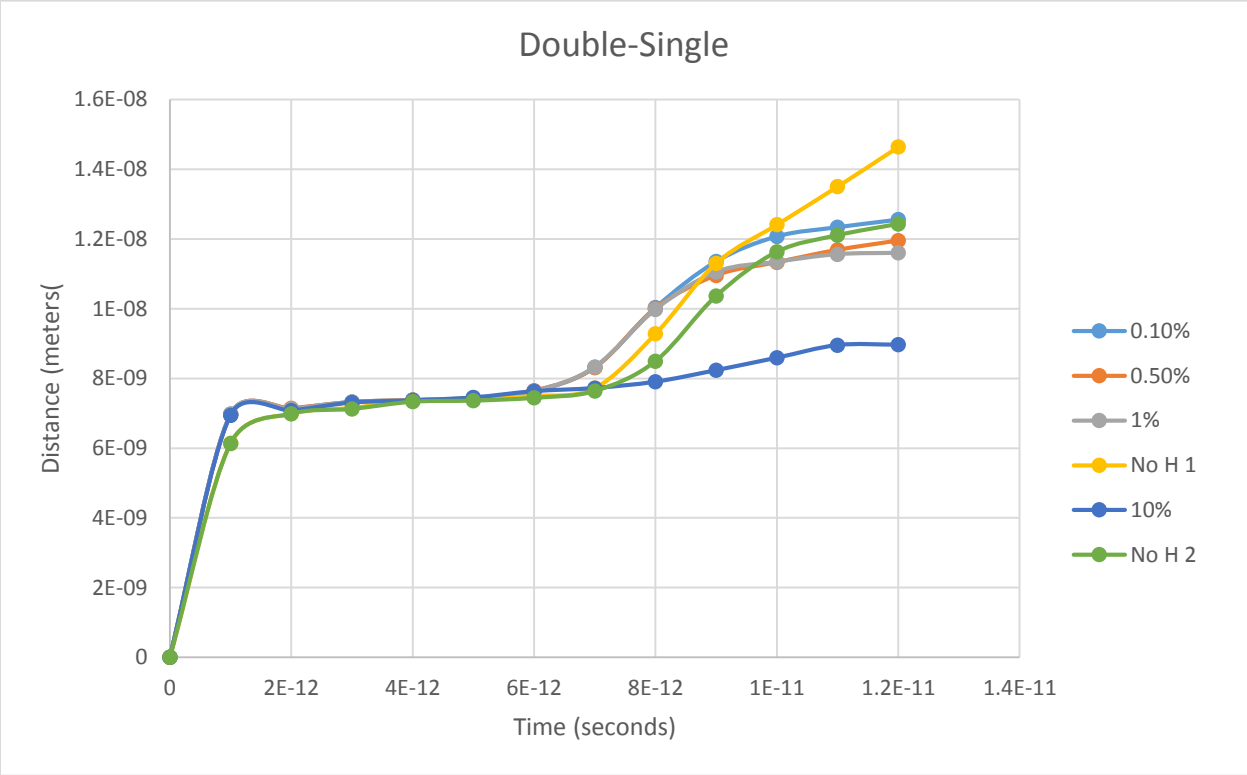


*Figure 9. 'Double-Single' D vs T graph comparing hydrogen concentrations.*

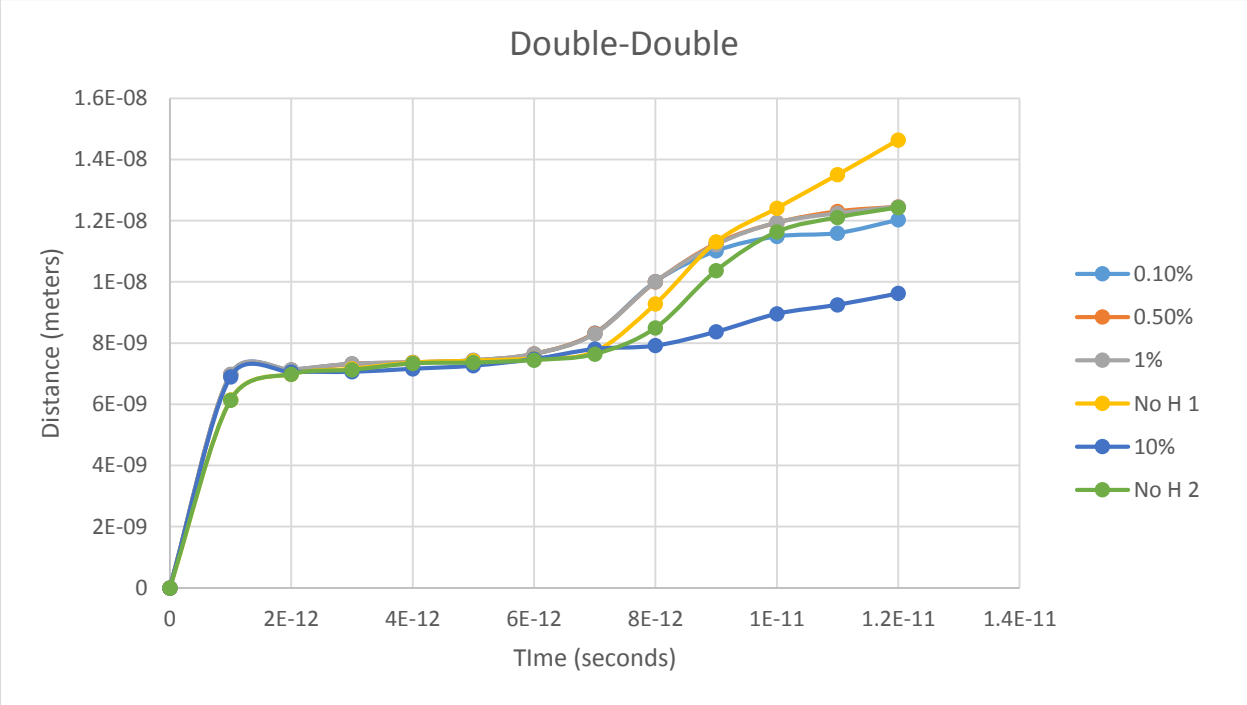


*Figure 10. 'Double-Double' D vs T graph comparing hydrogen concentrations.*

Figures 7-10 show a multi-stage non steady state propagation of the crack tip. Before the second time step, there is a clear difference in the velocity of the models with some hydrogen concentration and the models with no hydrogen present. The models with hydrogen have a higher crack tip velocity than the two different models without hydrogen. At this stage of the graph, there is a clear indication of the hydrogen enhanced decohesion (HEDE) mechanism. The fact that the crack tip velocity is higher for the hydrogen induced models shows that there is a reduction of the bonding strength between nickel atoms, thus presenting some evidence of the effect of hydrogen embrittlement in nickel via the HEDE mechanism. After this initial period of crack growth, the crack growth stalls as indicated by the flat position of the distance versus time curves. During this period, dislocations are nucleated from the crack tip. Eventually, the crack starts growing again, but the rate of crack propagation is hydrogen concentration dependent. This is evidence of the hydrogen enhanced localized plasticity (HELP) mechanism. The crack tip velocity for the hydrogen models seems to be lower in comparison to one of the nickel only models, but it is similar to the other nickel only model, which is likely due to statistical differences between the simulations in the way that dislocation nucleation occurs from the crack tip. As dislocations start to appear, the velocity of the crack tip slows down due to the "bottle-neck" effect caused by the generation of dislocations. One aspect to take into account, is the different behavior of the velocity curves for the hydrogen concentrations. The lower hydrogen concentrations seem to behave in a similar way as the nickel only models, meanwhile the 10% hydrogen concentration model shows quite a different behavior during the HELP phase of the graph. The crack tip does not grow as much more than the other models; this is due to the huge amount of dislocations being generated near the crack tip. This clearly shows that there is significant impact on the velocity of the crack tip by the amount of hydrogen located near it. Finally, it is acknowledged that dislocations nucleated from the crack

tip interact with the fixed boundaries used for loading and the free surface perpendicular to the crack propagation direction. In future studies, the role of the confinement of the dislocations by the simulation cell size on crack tip velocity must be further explored.

The models were also grouped by hydrogen concentrations, to study if there was a marked difference between regions. In other words, to see if the size of the region containing hydrogen atoms near the crack tip has some effect over how the crack behaves.

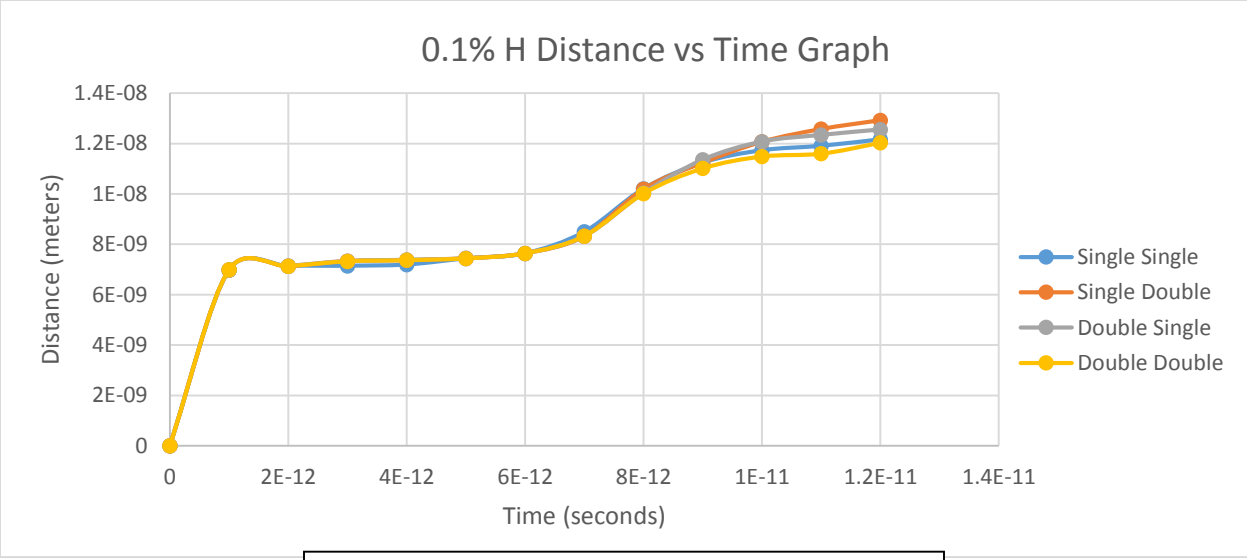


*Figure 11. 0.1% H D vs T Graph.*

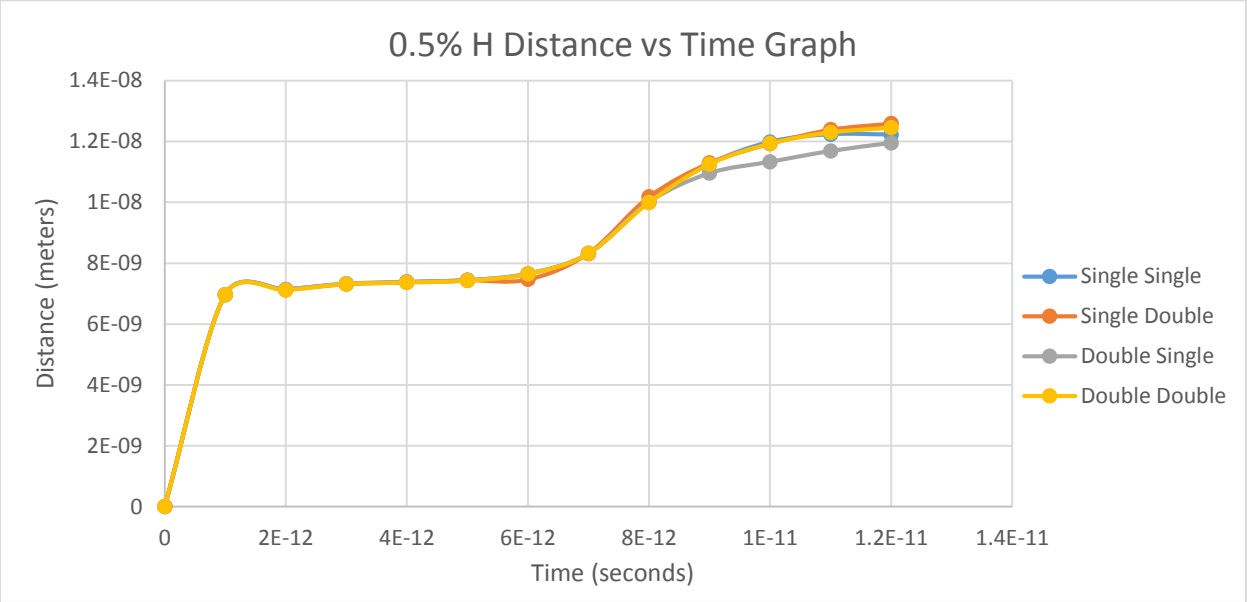


*Figure 12. 0.5% H D vs T Graph.*

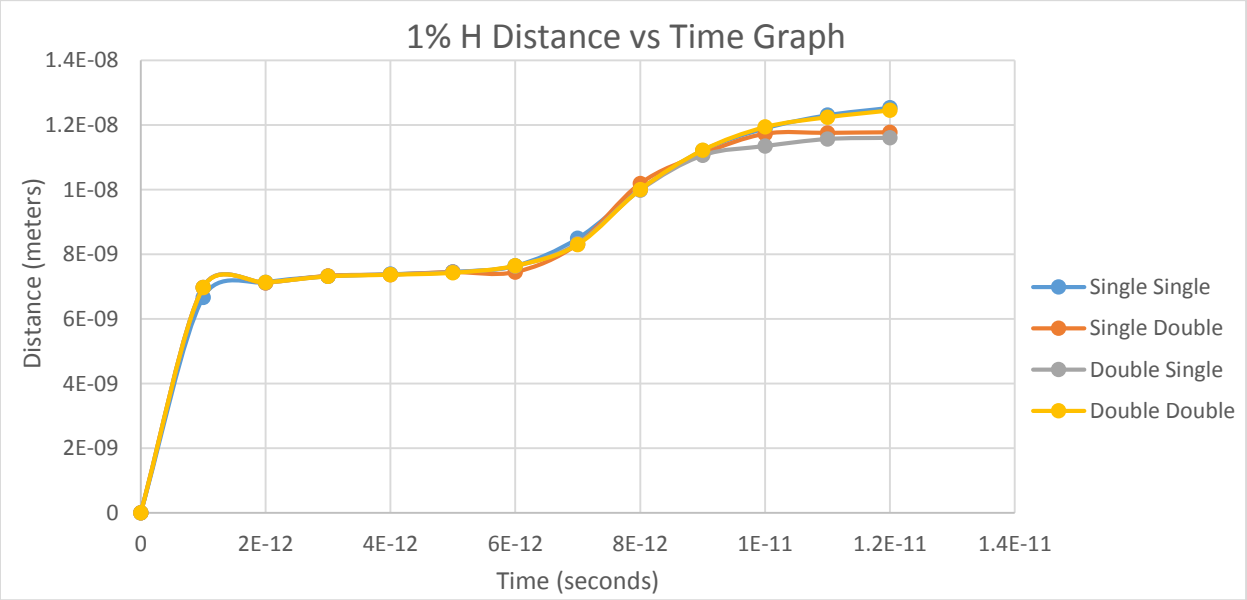


*Figure 13. 1% H D vs T Graph.*

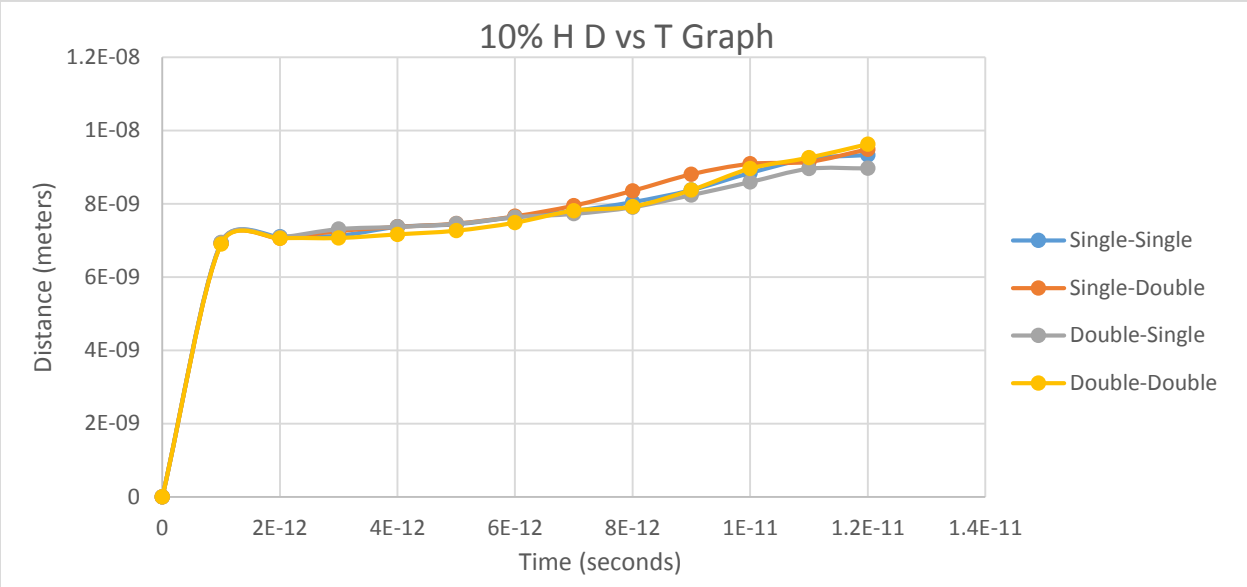


*Figure 14. 10% H D vs T Graph.*

Figures 11-14 show that even though there are minor differences between regions for the different hydrogen concentrations, there is no clear evidence of significant impact on the crack tip velocity caused by the size of the region that contains hydrogen atoms near the crack tip. All data tables used to generate the different distance versus time graphs can be found in Appendix A.

*Dislocation Nucleation*

To dig further into the HELP mechanism, the other important aspect studied in this research was how different concentrations of hydrogen and region sizes near the crack tip affect dislocation nucleation. As stated above, dislocations play a key role in the ductility of a material, and with the presence of hydrogen near the crack tip, dislocations are a critical part of the HELP mechanism, which at an atomic level would seem to work in favor of the material's ductility, but in the end causes the material to become more brittle at the macro scale. In order to analyze the dislocations in all models, OVITO's Dislocation Extraction Algorithm (DXA) was used. This algorithm helps provide a quantitative view of the plastic flow generated by the crack, by converting detected

dislocations into continuous lines [18]. By using the DXA, it was possible to know the length of all dislocations generated, and to compare this measurement between models with and without hydrogen. Note, usually dislocation line length is divided by the volume of the sample to compute a dislocation density, but this is not necessary here because the volume is consistent for all fracture models.

Figure 15 shows the comparison between one of the Ni only and Ni-H models ('Double-Double' region with 10% hydrogen) with the crack propagated before and after doing the DXA analysis. Note, Figure 15 shows crack propagation until dislocations nucleated from the crack tip start interacting with the fixed boundaries of the model. This means that the DXA analysis was performed at a different crack tip displacement for each model.

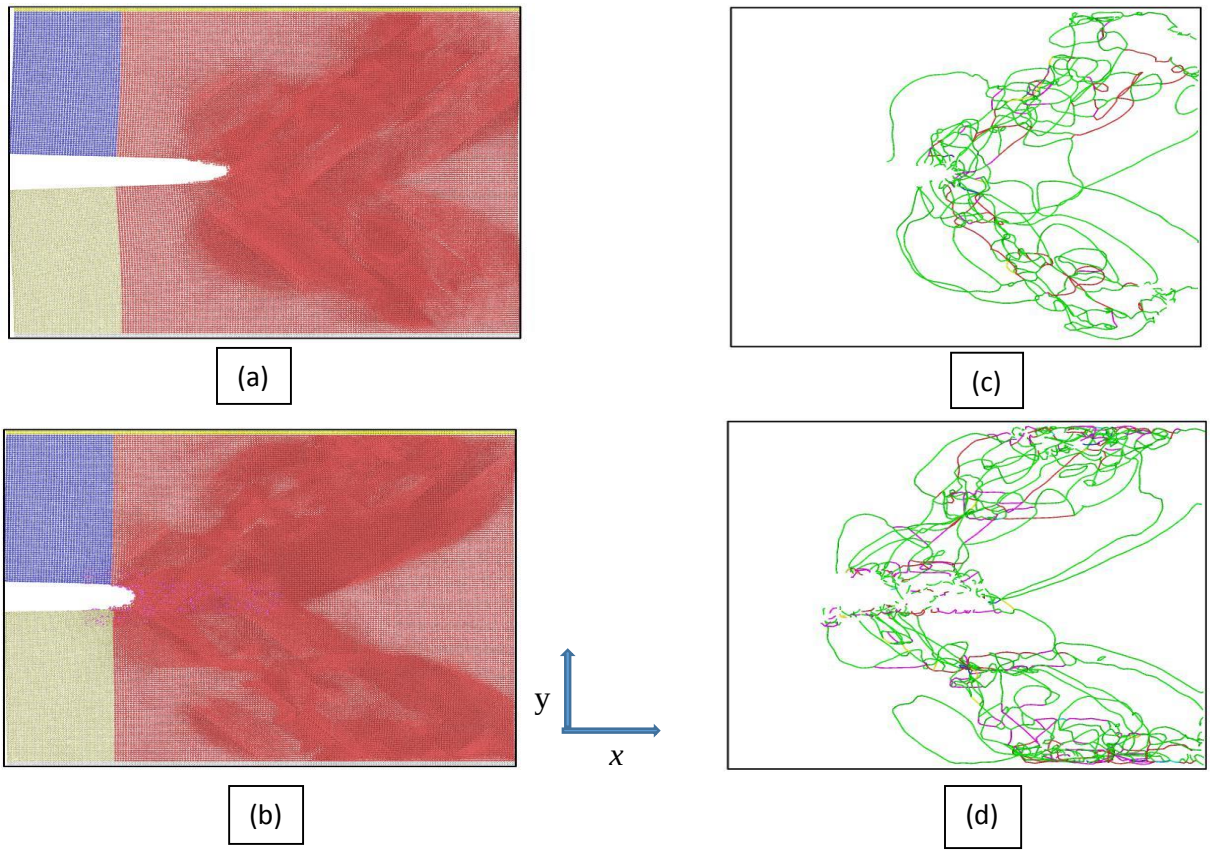


*Figure 15. (a) Ni only, (b) Ni-H, (c) Ni DXA analysis, (d) Ni-H DXA analysis.[13]*

In Figure 15 (a), (b), the shaded areas represent the dislocations generated. It is clear that the Ni-H model has more plastic flow than the Ni model. Figure 15 (c), (d) show the continuous dislocation core lines for both models. This qualitative view of the difference between the dislocation nucleation at the crack tip is now followed by a quantitative view. Data points for dislocation length for all models were calculated at the same crack tip displacement. Figure 16 shows the results for the length of dislocation lines for each of the models simulated.

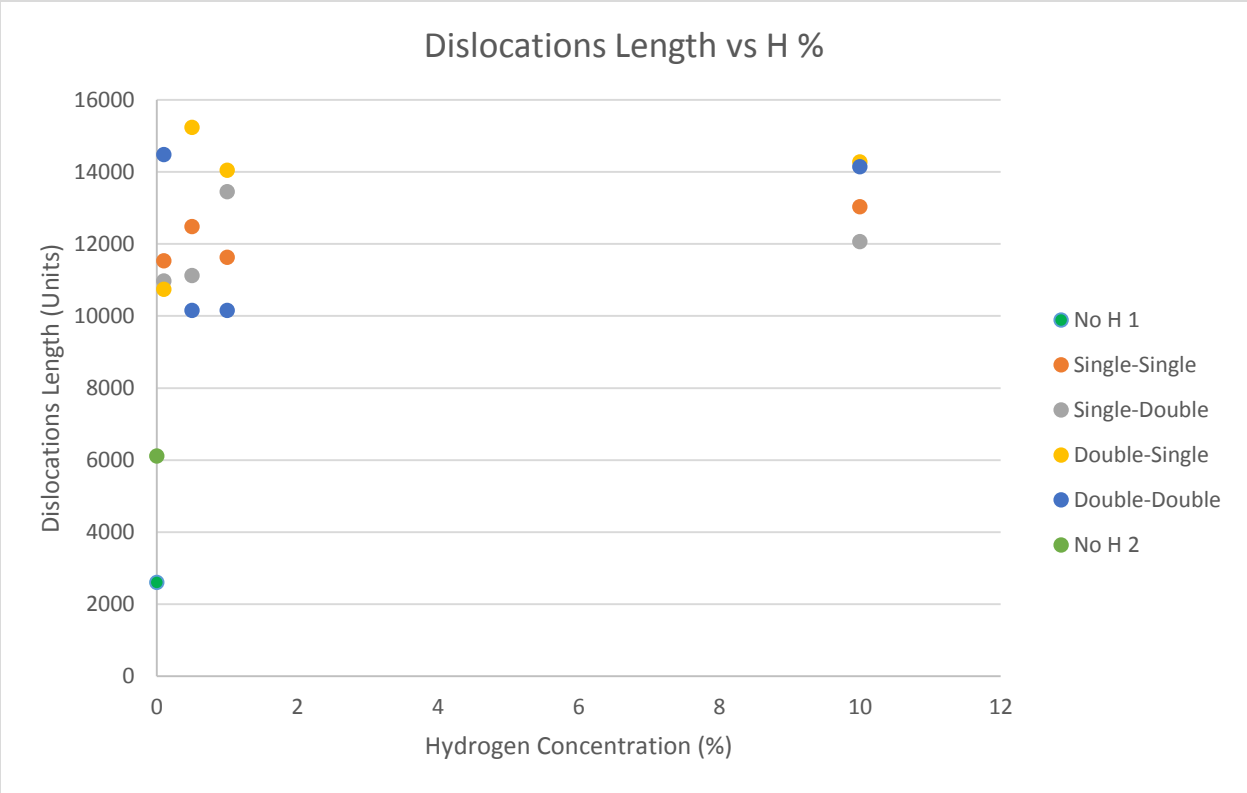


*Figure 16. Graph of the Dislocations Line Length vs Hydrogen Concentration.*

Figure 16 proves that there is a bigger production of dislocations at the crack tip from the various Ni-H models compared to the two Ni only models, thus showing the impact the presence of hydrogen near the crack tip has on dislocation nucleation via the HELP mechanism, another

way in which hydrogen embrittlement affects how a metal fracture at the atomic level. There are also differences between the different hydrogen concentrations and regions located. The ‘Double-Single’ region appears to be the one were more plastic flow is happening, especially at 0.5% hydrogen concentration. The dislocations length data tables can be found in Appendix A.

## Conclusions

After analyzing the data results from the single crystal 3D nickel model with and without hydrogen impurities, some important observations can be drawn.

1. The presence of hydrogen inside a nickel lattice has an impact on how it fractures at an atomic level.
2. Hydrogen concentration has a measurable impact on the crack tip velocity and on the dislocation nucleation at the crack tip. It is found that the initial crack tip velocity is 15% faster with hydrogen than without hydrogen in the model.
3. Different region sizes do not seem to have much of an effect on the velocity of the crack tip. Compared to each other, the cracks behave similar.
4. When analyzing the crack tip velocity, it is clear that different hydrogen embrittlement mechanisms are acting on the different stages of crack growth. These mechanisms are hydrogen enhanced decohesion and hydrogen enhance localized plasticity.
5. The presence of hydrogen enhances the formation and motion of dislocations, causing more plastic flow that then affects nickel by causing a brittle behavior of it at a macro scale.

Further studies on this topic may include running similar simulations in a larger model. This may allow for more crack propagation without generated dislocations reaching the fixed boundaries of the model. Another aspect to be studied, is crack propagating on different planes to explore the role of orientation of the crystal lattice.

**References**

[1] Unknown: *Tensile Properties.* NDT Resource Center. National Science Foundation. Accessed (March, 2016) https://www.nde-ed.org/EducationResources/CommunityCollege/Materials/Mechanical/Tensile.htm

[2] Daniel H. Herring: *Hydrogen Embrittlement*. The Heat Treat Doctor. The Herring Group, Inc. Accessed (Feb 27, 2015) http://www.heat-treat-doctor.com/documents/hydrogen%20embrittlement.pdf

[3] W.H. Johnson*: On some remarkable change produced in iron and steel by action of hydrogen and acids*. Proceedings of the Royal Society of London 23, 168-179 (1875).

[4] Dr.-Ing. Afrooz Barnoush*: Hydrogen Embrittlement*. Universitat des Saarlandes, 9-16 (Dec 1, 2011). Accessed (Feb 28, 2015) http://www.uni-saarland.de/fak8/wwm/research/phd_barnoush/hydrogen.pdf

[5] K.N. Solanski, D.K. Ward, D.J. Bammann: *A Nanoscale Study of Dislocation Nucleation at the Crack Tip in the Nickel-Hydrogen System*. The Minerals, Metals & Materials Society and ASM Internations 2010 (February 2011) DOI:10.1007/s11661-010-0451-8.

[6] J. Cwiek, A. Zielinski: *Mechanism of Hydrogen Enhanced-Cracking of High-Strength Steel Welded Joints*. Journal of Achievements in Materials and Manufacturing Engineering, Volume 18, Issue 1-2 (September-October 2006). Accessed (March, 2016). http://www.journalamme.org/papers_amme06/1178.pdf

[7] C. Beachem: *New Model for Hydrogen-Assisted Cracking-Hydrogen Embrittlement*. Metall. Trans. 3, 437-451 (1972).

[8] Steve Heminger: *Validity of Caltrans' Environmental Hydrogen Embrittlement Tests on Grade BD Anchor Rods in the SAS Span*. Toll Bridge Program Oversight Committee (TBPOC). (December 2, 2014). Accessed (March, 2016). http://www.sacbee.com/news/investigations/bay-bridge/article4254712.ece/BINARY/Validity%20of%20Caltrans'%20EHE%20Tests.pdf

[9] Unknown: *Theory of Molecular Dynamics Simulation*. Accessed (Mar 1, 2015). http://www.ch.embnet.org/MD_tutorial/pages/MD.Part1.html

[10] Unknown: *Interatomic Potential. Princeton University*. Accessed (March, 2016). https://www.princeton.edu/~maelabs/mae324/glos324/potential.htm

[11] LAMMPS: *Molecular Dynamics Simulator*. Accessed (Mar 1, 2015). http://lammps.sandia.gov/

[12] OVITO: *Open Visualization Tool*. Accessed (Mar 1, 2015). http://www.ovito.org/

[13] A. Stukowski, *Modellin Simul. Mater. Sci. Eng.* 18, 015012 (2010).

[14] Arkansas High Performance Computing Center. Accessed (Mar 2, 2015). http://hpc.uark.edu/

[15] SM Foiles et al, PRB, 33, 7983 (1986).

[16] James E. Angelo, Neville R Moody, Michael I Baskes. *Trapping of Hydrogen to Lattice Defects in Nickel*. Modelling and Simulation in Materials Science & Engineering, Vol.3, pp.289-307 (1995).

[17] LAMMPS: *Minimize Command*. Accessed (March, 2016). http://lammps.sandia.gov/doc/minimize.html

[18] A. Stukowski: *Dislocation Extraction Algorithm (DXA).* Accessed (March, 2016). http://dxa.ovito.org/

[19] H.K. Birnbaum and P. Sofronis: *Mater. Sci. Eng. A., Struct. Mater., Prop. Microstruct. Process*, 1993, vol. A176, pp. 191-202.

[20] I.M. Robertson, H.K. Birnbaum, and P. Sofronis: in *Dislocations in Solids*, J.P. Hirth and L. Kubin, eds., Elsevier, New York, 2009, vol19, pp.249-93.

[21] I.M. Robertson and H.K Birnbaum: *Acta Metall*., 1986, vol. 34, pp. 353-66.

[22] T. Tabata and H.K. Birnbaum: *Scripta Metall*., 1984, vol. 17, pp. 947-50.

## Appendix A

*Data Tables*

| No H 1 | | | |
|---|---|---|---|
| Distance (Angstroms) | Distance (m) | Time (picoseconds) | Time (seconds) |
| 0 | 0 | 0 | 0 |
| 61.3965 | 6.13965E-09 | 1 | 1E-12 |
| 69.8544 | 6.98544E-09 | 2 | 2E-12 |
| 71.5736 | 7.15736E-09 | 3 | 3E-12 |
| 73.6196 | 7.36196E-09 | 4 | 4E-12 |
| 74.2352 | 7.42352E-09 | 5 | 5E-12 |
| 74.9658 | 7.49658E-09 | 6 | 6E-12 |
| 77.2315 | 7.72315E-09 | 7 | 7E-12 |
| 92.8018 | 9.28018E-09 | 8 | 8E-12 |
| 113.052 | 1.13052E-08 | 9 | 9E-12 |
| 124.116 | 1.24116E-08 | 10 | 1E-11 |
| 135.041 | 1.35041E-08 | 11 | 1.1E-11 |
| 146.405 | 1.46405E-08 | 12 | 1.2E-11 |

*Table 3. First nickel only model distance traveled by crack.*

| No H 2 | | | |
|---|---|---|---|
| Distance (Angstroms) | Distance (m) | Time (picoseconds) | Time (seconds) |
| 0 | 0 | 0 | 0 |
| 61.3045 | 6.13045E-09 | 1 | 1E-12 |
| 69.8456 | 6.98456E-09 | 2 | 2E-12 |
| 71.2576 | 7.12576E-09 | 3 | 3E-12 |
| 73.3211 | 7.33211E-09 | 4 | 4E-12 |
| 73.6329 | 7.36329E-09 | 5 | 5E-12 |
| 74.4355 | 7.44355E-09 | 6 | 6E-12 |
| 76.3954 | 7.63954E-09 | 7 | 7E-12 |
| 84.9584 | 8.49584E-09 | 8 | 8E-12 |
| 103.682 | 1.03682E-08 | 9 | 9E-12 |
| 116.323 | 1.16323E-08 | 10 | 1E-11 |
| 121.067 | 1.21067E-08 | 11 | 1.1E-11 |
| 124.314 | 1.24314E-08 | 12 | 1.2E-11 |

*Table 4. Second nickel only model distance traveled by crack*

| 0.10% | | | |
|---|---|---|---|
| Distance (Angstroms) | Distance (m) | Time (picoseconds) | Time (seconds) |
| 0 | 0 | 0 | 0 |
| 69.735 | 6.9735E-09 | 1 | 1E-12 |
| 71.3343 | 7.13343E-09 | 2 | 2E-12 |
| 71.4576 | 7.14576E-09 | 3 | 3E-12 |
| 71.9404 | 7.19404E-09 | 4 | 4E-12 |
| 74.3695 | 7.43695E-09 | 5 | 5E-12 |
| 76.3927 | 7.63927E-09 | 6 | 6E-12 |
| 84.962 | 8.4962E-09 | 7 | 7E-12 |
| 102.081 | 1.02081E-08 | 8 | 8E-12 |
| 112.443 | 1.12443E-08 | 9 | 9E-12 |
| 117.332 | 1.17332E-08 | 10 | 1E-11 |
| 119.092 | 1.19092E-08 | 11 | 1.1E-11 |
| 121.646 | 1.21646E-08 | 12 | 1.2E-11 |

*Table 5. 'Single-Single' with 0.1% H model distance traveled by crack.*

| 0.50% | | | |
|---|---|---|---|
| Distance (Angstroms) | Distance (m) | Time (picoseconds) | Time (seconds) |
| 0 | 0 | 0 | 0 |
| 69.6952 | 6.96952E-09 | 1 | 1E-12 |
| 71.3514 | 7.13514E-09 | 2 | 2E-12 |
| 73.2354 | 7.32354E-09 | 3 | 3E-12 |
| 73.8168 | 7.38168E-09 | 4 | 4E-12 |
| 74.425 | 7.4425E-09 | 5 | 5E-12 |
| 76.5428 | 7.65428E-09 | 6 | 6E-12 |
| 83.1795 | 8.31795E-09 | 7 | 7E-12 |
| 100.171 | 1.00171E-08 | 8 | 8E-12 |
| 112.594 | 1.12594E-08 | 9 | 9E-12 |
| 119.85 | 1.1985E-08 | 10 | 1E-11 |
| 122.37 | 1.2237E-08 | 11 | 1.1E-11 |
| 122.27 | 1.2227E-08 | 12 | 1.2E-11 |

*Table 6. 'Single-Single' with 0.5% H model distance traveled by crack.*

| 1% | | | |
|---|---|---|---|
| Distance (Angstroms) | Distance (m) | Time (picoseconds) | Time (seconds) |
| 0 | 0 | 0 | 0 |
| 66.6659 | 6.66659E-09 | 1 | 1E-12 |
| 71.319 | 7.1319E-09 | 2 | 2E-12 |
| 73.2002 | 7.32002E-09 | 3 | 3E-12 |
| 73.8251 | 7.38251E-09 | 4 | 4E-12 |
| 74.5662 | 7.45662E-09 | 5 | 5E-12 |
| 76.405 | 7.6405E-09 | 6 | 6E-12 |
| 84.9034 | 8.49034E-09 | 7 | 7E-12 |
| 100.081 | 1.00081E-08 | 8 | 8E-12 |
| 112.084 | 1.12084E-08 | 9 | 9E-12 |
| 118.929 | 1.18929E-08 | 10 | 1E-11 |
| 123.007 | 1.23007E-08 | 11 | 1.1E-11 |
| 125.299 | 1.25299E-08 | 12 | 1.2E-11 |

*Table 7. 'Single-Single' with 1% H model distance traveled by crack.*

| 10% | | | |
|---|---|---|---|
| Distance (Angstroms) | Distance (m) | Time (picoseconds) | Time (seconds) |
| 0 | 0 | 0 | 0 |
| 69.3525 | 6.93525E-09 | 1 | 1E-12 |
| 70.9544 | 7.09544E-09 | 2 | 2E-12 |
| 71.2663 | 7.12663E-09 | 3 | 3E-12 |
| 73.6798 | 7.36798E-09 | 4 | 4E-12 |
| 74.387 | 7.4387E-09 | 5 | 5E-12 |
| 76.3452 | 7.63452E-09 | 6 | 6E-12 |
| 78.044 | 7.8044E-09 | 7 | 7E-12 |
| 80.4389 | 8.04389E-09 | 8 | 8E-12 |
| 83.7259 | 8.37259E-09 | 9 | 9E-12 |
| 88.399 | 8.8399E-09 | 10 | 1E-11 |
| 92.2831 | 9.22831E-09 | 11 | 1.1E-11 |
| 93.2978 | 9.32978E-09 | 12 | 1.2E-11 |

*Table 8. 'Single-Single' with 10% H model distance traveled by crack.*

| 0.10% | | | |
|---|---|---|---|
| Distance (Angstroms) | Distance (m) | Time (picoseconds) | Time (seconds) |
| 0 | 0 | 0 | 0 |
| 69.8377 | 6.98377E-09 | 1 | 1E-12 |
| 71.2647 | 7.12647E-09 | 2 | 2E-12 |
| 73.3099 | 7.33099E-09 | 3 | 3E-12 |
| 73.6953 | 7.36953E-09 | 4 | 4E-12 |
| 74.4283 | 7.44283E-09 | 5 | 5E-12 |
| 76.4025 | 7.64025E-09 | 6 | 6E-12 |
| 83.1727 | 8.31727E-09 | 7 | 7E-12 |
| 101.939 | 1.01939E-08 | 8 | 8E-12 |
| 112.365 | 1.12365E-08 | 9 | 9E-12 |
| 120.695 | 1.20695E-08 | 10 | 1E-11 |
| 125.76 | 1.2576E-08 | 11 | 1.1E-11 |
| 129.275 | 1.29275E-08 | 12 | 1.2E-11 |

*Table 9. 'Single-Double' with 0.1% H model distance traveled by crack.*

| 0.50% | | | |
|---|---|---|---|
| Distance (Angstroms) | Distance (m) | Time (picoseconds) | Time (seconds) |
| 0 | 0 | 0 | 0 |
| 69.6786 | 6.96786E-09 | 1 | 1E-12 |
| 71.334 | 7.1334E-09 | 2 | 2E-12 |
| 73.1545 | 7.31545E-09 | 3 | 3E-12 |
| 73.7583 | 7.37583E-09 | 4 | 4E-12 |
| 74.4248 | 7.44248E-09 | 5 | 5E-12 |
| 74.6689 | 7.46689E-09 | 6 | 6E-12 |
| 83.2566 | 8.32566E-09 | 7 | 7E-12 |
| 101.791 | 1.01791E-08 | 8 | 8E-12 |
| 112.953 | 1.12953E-08 | 9 | 9E-12 |
| 119.275 | 1.19275E-08 | 10 | 1E-11 |
| 123.897 | 1.23897E-08 | 11 | 1.1E-11 |
| 125.913 | 1.25913E-08 | 12 | 1.2E-11 |

*Table 10. 'Single-Double' with 0.5% H model distance traveled by crack.*

| 1% | | | |
|---|---|---|---|
| Distance (Angstrongs) | Distance (m) | Time (picoseconds) | Time (seconds) |
| 0 | 0 | 0 | 0 |
| 69.759 | 6.9759E-09 | 1 | 1E-12 |
| 71.1345 | 7.11345E-09 | 2 | 2E-12 |
| 73.3173 | 7.33173E-09 | 3 | 3E-12 |
| 73.7161 | 7.37161E-09 | 4 | 4E-12 |
| 74.4721 | 7.44721E-09 | 5 | 5E-12 |
| 74.4895 | 7.44895E-09 | 6 | 6E-12 |
| 83.1057 | 8.31057E-09 | 7 | 7E-12 |
| 101.829 | 1.01829E-08 | 8 | 8E-12 |
| 110.977 | 1.10977E-08 | 9 | 9E-12 |
| 117.22 | 1.1722E-08 | 10 | 1E-11 |
| 117.51 | 1.1751E-08 | 11 | 1.1E-11 |
| 117.694 | 1.17694E-08 | 12 | 1.2E-11 |

*Table 11. 'Single-Double' with 1% H model distance traveled by crack.*

| 10% | | | |
|---|---|---|---|
| Distance (Angstroms) | Distance (m) | Time (picoseconds) | Time (seconds) |
| 0 | 0 | 0 | 0 |
| 69.1117 | 6.91117E-09 | 1 | 1E-12 |
| 70.536 | 7.0536E-09 | 2 | 2E-12 |
| 72.5127 | 7.25127E-09 | 3 | 3E-12 |
| 73.6535 | 7.36535E-09 | 4 | 4E-12 |
| 74.5544 | 7.45544E-09 | 5 | 5E-12 |
| 76.5437 | 7.65437E-09 | 6 | 6E-12 |
| 79.4586 | 7.94586E-09 | 7 | 7E-12 |
| 83.5101 | 8.35101E-09 | 8 | 8E-12 |
| 88.0156 | 8.80156E-09 | 9 | 9E-12 |
| 90.8648 | 9.08648E-09 | 10 | 1E-11 |
| 91.4167 | 9.14167E-09 | 11 | 1.1E-11 |
| 94.8465 | 9.48465E-09 | 12 | 1.2E-11 |

*Table 12. 'Single-Double' with 10% H model distance traveled by crack.*

| 0.10% | | | |
|---|---|---|---|
| Distance (Angstroms) | Distance (m) | Time (picoseconds) | Time (seconds) |
| 0 | 0 | 0 | 0 |
| 69.7449 | 6.97449E-09 | 1 | 1E-12 |
| 71.3805 | 7.13805E-09 | 2 | 2E-12 |
| 73.2792 | 7.32792E-09 | 3 | 3E-12 |
| 73.7897 | 7.37897E-09 | 4 | 4E-12 |
| 74.3949 | 7.43949E-09 | 5 | 5E-12 |
| 76.361 | 7.6361E-09 | 6 | 6E-12 |
| 83.1693 | 8.31693E-09 | 7 | 7E-12 |
| 100.332 | 1.00332E-08 | 8 | 8E-12 |
| 113.571 | 1.13571E-08 | 9 | 9E-12 |
| 120.745 | 1.20745E-08 | 10 | 1E-11 |
| 123.389 | 1.23389E-08 | 11 | 1.1E-11 |
| 125.547 | 1.25547E-08 | 12 | 1.2E-11 |

*Table 13. 'Double-Single' with 0.1% H model distance traveled by crack.*

| 0.50% | | | |
|---|---|---|---|
| Distance (Angstroms) | Distance (m) | Time (picoseconds) | Time (seconds) |
| 0 | 0 | 0 | 0 |
| 69.6977 | 6.96977E-09 | 1 | 1E-12 |
| 71.3938 | 7.13938E-09 | 2 | 2E-12 |
| 73.1998 | 7.31998E-09 | 3 | 3E-12 |
| 73.7976 | 7.37976E-09 | 4 | 4E-12 |
| 74.378 | 7.4378E-09 | 5 | 5E-12 |
| 76.4823 | 7.64823E-09 | 6 | 6E-12 |
| 83.1209 | 8.31209E-09 | 7 | 7E-12 |
| 100.1 | 1.001E-08 | 8 | 8E-12 |
| 109.572 | 1.09572E-08 | 9 | 9E-12 |
| 113.316 | 1.13316E-08 | 10 | 1E-11 |
| 116.863 | 1.16863E-08 | 11 | 1.1E-11 |
| 119.533 | 1.19533E-08 | 12 | 1.2E-11 |

*Table 14. 'Double-Single' with 0.5% H model distance traveled by crack.*

| 1% | | | |
|---|---|---|---|
| Distance (Angstroms) | Distance (m) | Time (picoseconds) | Time (seconds) |
| 0 | 0 | 0 | 0 |
| 69.7561 | 6.97561E-09 | 1 | 1E-12 |
| 71.2102 | 7.12102E-09 | 2 | 2E-12 |
| 73.182 | 7.3182E-09 | 3 | 3E-12 |
| 73.7736 | 7.37736E-09 | 4 | 4E-12 |
| 74.436 | 7.4436E-09 | 5 | 5E-12 |
| 76.3332 | 7.63332E-09 | 6 | 6E-12 |
| 83.3042 | 8.33042E-09 | 7 | 7E-12 |
| 99.8036 | 9.98036E-09 | 8 | 8E-12 |
| 110.542 | 1.10542E-08 | 9 | 9E-12 |
| 113.432 | 1.13432E-08 | 10 | 1E-11 |
| 115.619 | 1.15619E-08 | 11 | 1.1E-11 |
| 115.999 | 1.15999E-08 | 12 | 1.2E-11 |

*Table 15. 'Double-Single' with 1% H model distance traveled by crack.*

| 10% | | | |
|---|---|---|---|
| Distance (Angstroms) | Distance (m) | Time (picoseconds) | Time (seconds) |
| 0 | 0 | 0 | 0 |
| 69.4476 | 6.94476E-09 | 1 | 1E-12 |
| 70.7932 | 7.07932E-09 | 2 | 2E-12 |
| 73.0896 | 7.30896E-09 | 3 | 3E-12 |
| 73.689 | 7.3689E-09 | 4 | 4E-12 |
| 74.5464 | 7.45464E-09 | 5 | 5E-12 |
| 76.338 | 7.6338E-09 | 6 | 6E-12 |
| 77.2482 | 7.72482E-09 | 7 | 7E-12 |
| 79.0607 | 7.90607E-09 | 8 | 8E-12 |
| 82.3715 | 8.23715E-09 | 9 | 9E-12 |
| 85.9419 | 8.59419E-09 | 10 | 1E-11 |
| 89.5593 | 8.95593E-09 | 11 | 1.1E-11 |
| 89.673 | 8.9673E-09 | 12 | 1.2E-11 |

*Table 16. 'Double-Single' with 10% H model distance traveled by crack.*

| 0.10% | | | |
|---|---|---|---|
| Distance (Angstroms) | Distance (m) | Time (picoseconds) | Time (seconds) |
| 0 | 0 | 0 | 0 |
| 69.8327 | 6.98327E-09 | 1 | 1E-12 |
| 71.284 | 7.1284E-09 | 2 | 2E-12 |
| 73.2105 | 7.32105E-09 | 3 | 3E-12 |
| 73.6505 | 7.36505E-09 | 4 | 4E-12 |
| 74.3857 | 7.43857E-09 | 5 | 5E-12 |
| 76.3968 | 7.63968E-09 | 6 | 6E-12 |
| 83.2699 | 8.32699E-09 | 7 | 7E-12 |
| 100.137 | 1.00137E-08 | 8 | 8E-12 |
| 110.134 | 1.10134E-08 | 9 | 9E-12 |
| 114.846 | 1.14846E-08 | 10 | 1E-11 |
| 115.964 | 1.15964E-08 | 11 | 1.1E-11 |
| 120.268 | 1.20268E-08 | 12 | 1.2E-11 |

*Table 17. 'Double-Double' with 0.1% H model distance traveled by crack.*

| 0.50% | | | |
|---|---|---|---|
| Distance (Angstroms) | Distance (m) | Time (picoseconds) | Time (seconds) |
| 0 | 0 | 0 | 0 |
| 69.6661 | 6.96661E-09 | 1 | 1E-12 |
| 71.1404 | 7.11404E-09 | 2 | 2E-12 |
| 73.1674 | 7.31674E-09 | 3 | 3E-12 |
| 73.6903 | 7.36903E-09 | 4 | 4E-12 |
| 74.3052 | 7.43052E-09 | 5 | 5E-12 |
| 76.4736 | 7.64736E-09 | 6 | 6E-12 |
| 83.1974 | 8.31974E-09 | 7 | 7E-12 |
| 99.9978 | 9.99978E-09 | 8 | 8E-12 |
| 112.554 | 1.12554E-08 | 9 | 9E-12 |
| 119.351 | 1.19351E-08 | 10 | 1E-11 |
| 123.022 | 1.23022E-08 | 11 | 1.1E-11 |
| 124.55 | 1.2455E-08 | 12 | 1.2E-11 |

*Table 18. 'Double-Double' with 0.5% H model distance traveled by crack.*

| 1% | | | |
|---|---|---|---|
| Distance (Angstroms) | Distance (m) | Time (picoseconds) | Time (seconds) |
| 0 | 0 | 0 | 0 |
| 69.6661 | 6.96661E-09 | 1 | 1E-12 |
| 71.2654 | 7.12654E-09 | 2 | 2E-12 |
| 73.1674 | 7.31674E-09 | 3 | 3E-12 |
| 73.6903 | 7.36903E-09 | 4 | 4E-12 |
| 74.3052 | 7.43052E-09 | 5 | 5E-12 |
| 76.4736 | 7.64736E-09 | 6 | 6E-12 |
| 83.0082 | 8.30082E-09 | 7 | 7E-12 |
| 99.9978 | 9.99978E-09 | 8 | 8E-12 |
| 112.184 | 1.12184E-08 | 9 | 9E-12 |
| 119.351 | 1.19351E-08 | 10 | 1E-11 |
| 122.398 | 1.22398E-08 | 11 | 1.1E-11 |
| 124.516 | 1.24516E-08 | 12 | 1.2E-11 |

*Table 19. 'Double-Double' with 1% H model distance traveled by crack*

| 10% | | | |
|---|---|---|---|
| Distance (Angstroms) | Distance (m) | Time (picoseconds) | Time (seconds) |
| 0 | 0 | 0 | 0 |
| 69.0136 | 6.90136E-09 | 1 | 1E-12 |
| 70.5254 | 7.05254E-09 | 2 | 2E-12 |
| 70.6163 | 7.06163E-09 | 3 | 3E-12 |
| 71.6152 | 7.16152E-09 | 4 | 4E-12 |
| 72.6165 | 7.26165E-09 | 5 | 5E-12 |
| 74.8009 | 7.48009E-09 | 6 | 6E-12 |
| 78.0861 | 7.80861E-09 | 7 | 7E-12 |
| 79.1828 | 7.91828E-09 | 8 | 8E-12 |
| 83.7219 | 8.37219E-09 | 9 | 9E-12 |
| 89.5703 | 8.95703E-09 | 10 | 1E-11 |
| 92.541 | 9.2541E-09 | 11 | 1.1E-11 |
| 96.2335 | 9.62335E-09 | 12 | 1.2E-11 |

*Table 20. 'Double-Double' with 10% H model distance traveled by crack.*

| Single-Single | |
|---|---|
| Hydrogen Concentration (%) | Length (Units) |
| 0.1 | 11531.7005 |
| 0.5 | 12483.4 |
| 1 | 11630.5 |
| 10 | 13034.4 |

*Table 21. 'Single-Single' Dislocations length for different hydrogen concentrations.*

| Single-Double | |
|---|---|
| Hydrogen Concentration (%) | Length (Units) |
| 0.1 | 10969.6 |
| 0.5 | 11122.2 |
| 1 | 13453.1 |
| 10 | 12061.9 |

*Table 22. 'Single-Double' Dislocations length for different hydrogen concentrations.*

| Double-Single | |
|---|---|
| Hydrogen Concentration (%) | Length (Units) |
| 0.1 | 10738.2 |
| 0.5 | 15233.3 |
| 1 | 14049.3 |
| 10 | 14273.9 |

*Table 23. 'Double-Single' Dislocations length for different hydrogen concentrations.*

| Double-Double | |
|---|---|
| Hydrogen Concentration (%) | Length (Units) |
| 0.1 | 14483.6 |
| 0.5 | 10156.8 |
| 1 | 10156.8 |
| 10 | 14140 |

*Table 24. 'Double-Double' Dislocations length for different hydrogen concentrations.*

| No H | |
|---|---|
| Nickel IP Used | Length (Units) |
| 1 | 2603.16 |
| 2 | 6111.52 |

*Table 25. Nickel Models Dislocations length.*

## Appendix B

*Snapshots of crack propagating in each of the models with hydrogen. Hydrogen atoms are enlarged for viewing purposes.*

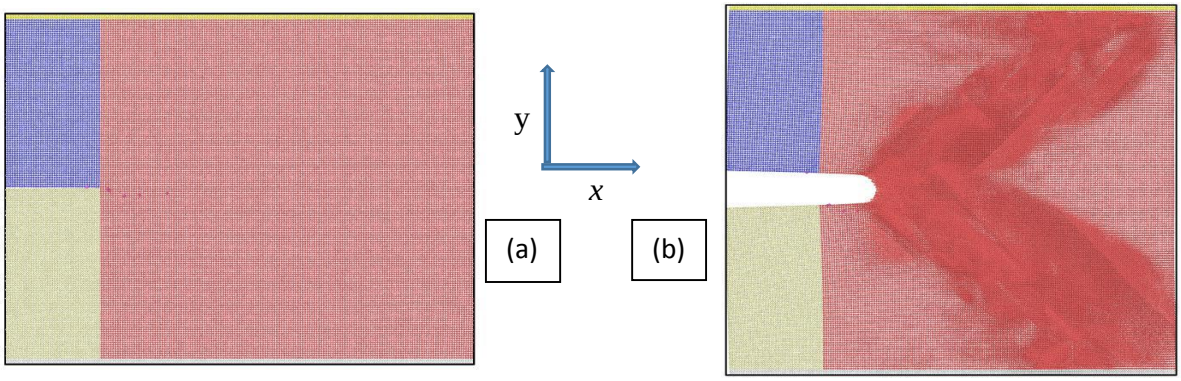


*Figure 17. 'Single-Single' with 0.1% hydrogen (a) Crack at T=0 ps, (b) Crack at T=12 ps*

`

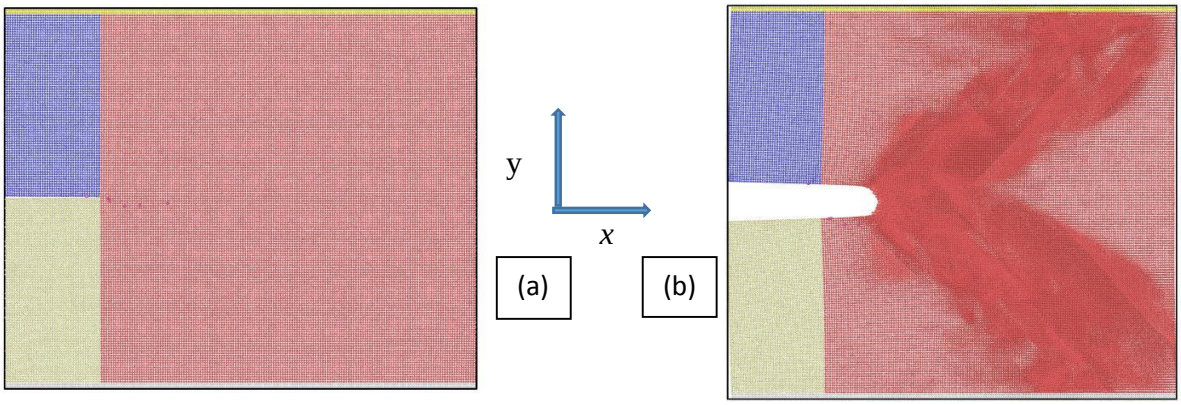


*Figure 18. 'Single-Single' with 0.5% hydrogen (a) Crack at T=0 ps, (b) Crack at T=12 ps*

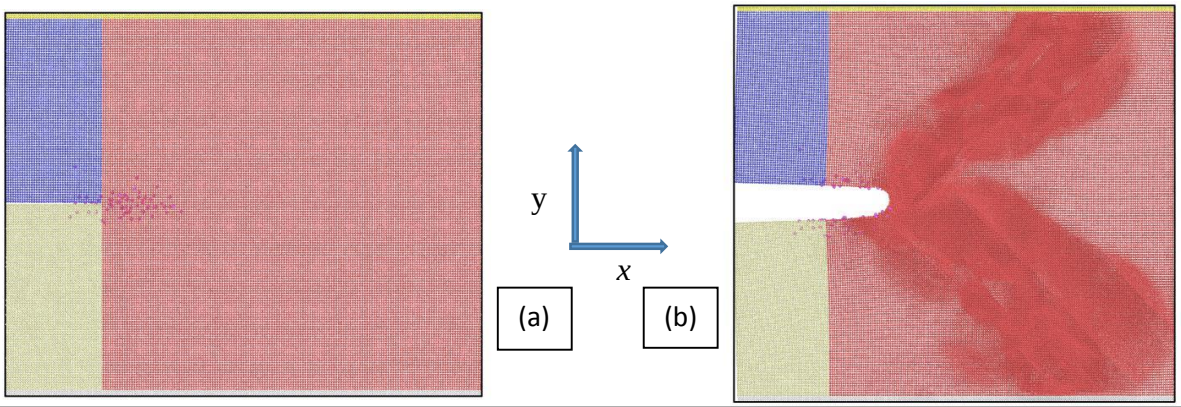


*Figure 19. 'Single-Single' with 1% hydrogen (a) Crack at T=0 ps, (b) Crack at T=12 ps*

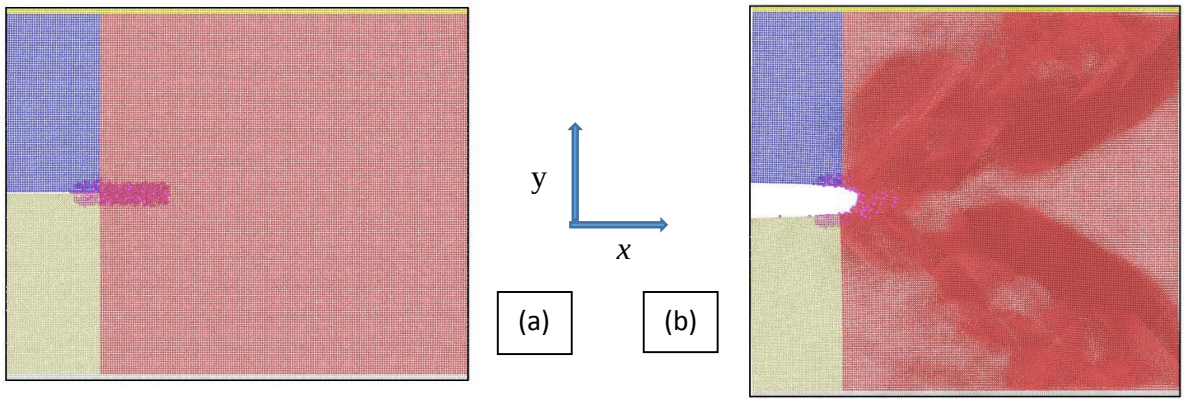


*Figure 20. 'Single-Single' with 10% hydrogen (a) Crack at T=0 ps, (b) Crack at T=12 ps*

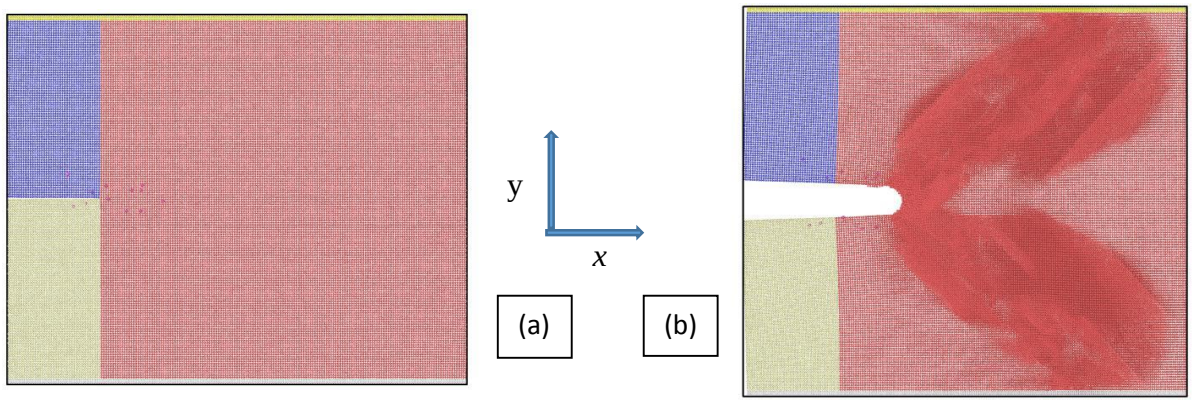


*Figure 21. 'Single-Double' with 0.1% hydrogen (a) Crack at T=0 ps, (b) Crack at T=12 ps*

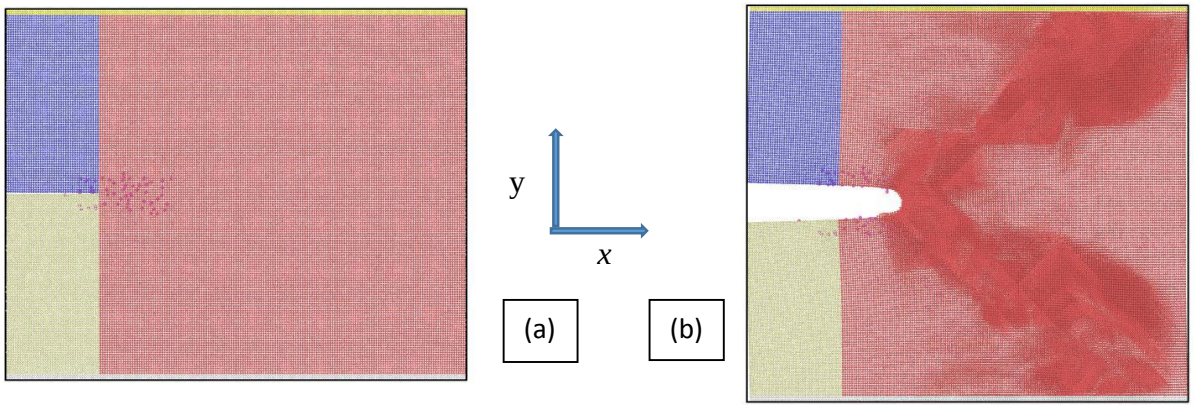


*Figure 22. 'Single-Double' with 0.5% hydrogen (a) Crack at T=0 ps, (b) Crack at T=12 ps*

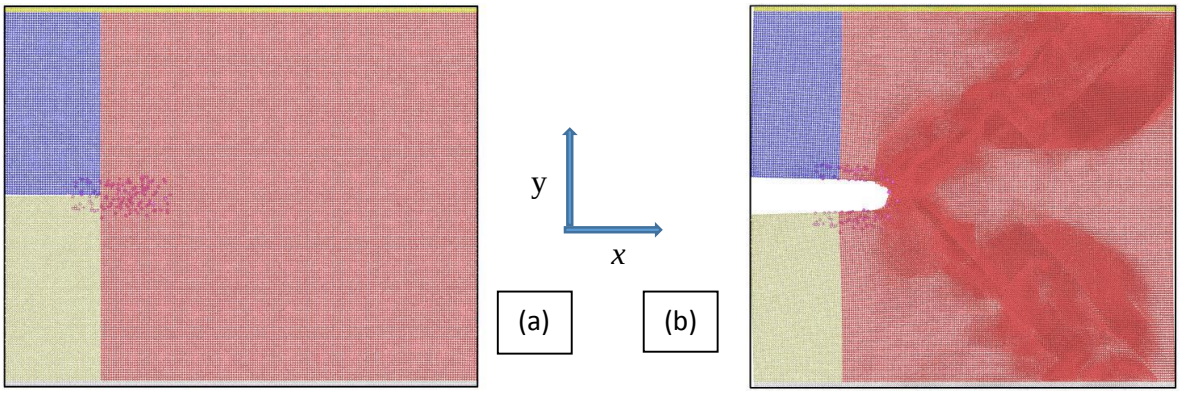


*Figure 23. 'Single-Double' with 1% hydrogen (a) Crack at T=0 ps, (b) Crack at T=12 ps*

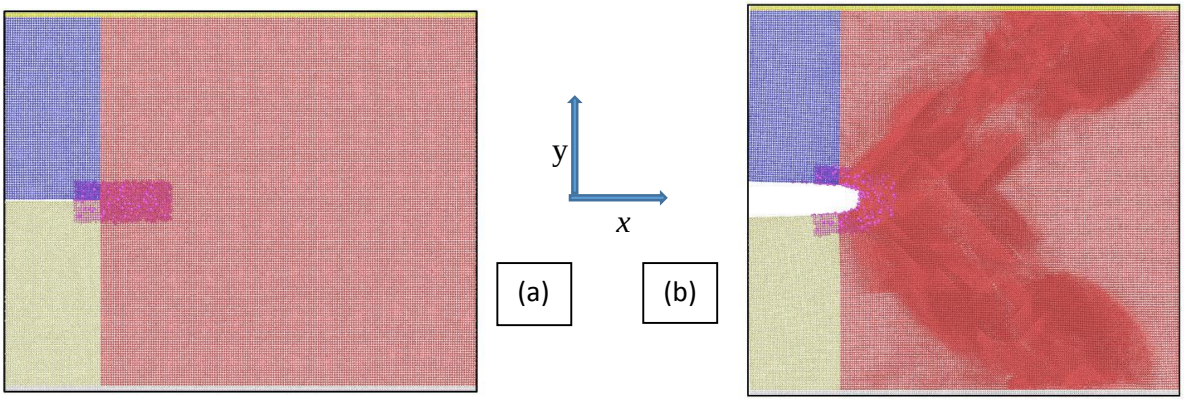


*Figure 24. 'Single-Double' with 1% hydrogen (a) Crack at T=0 ps, (b) Crack at T=12 ps*

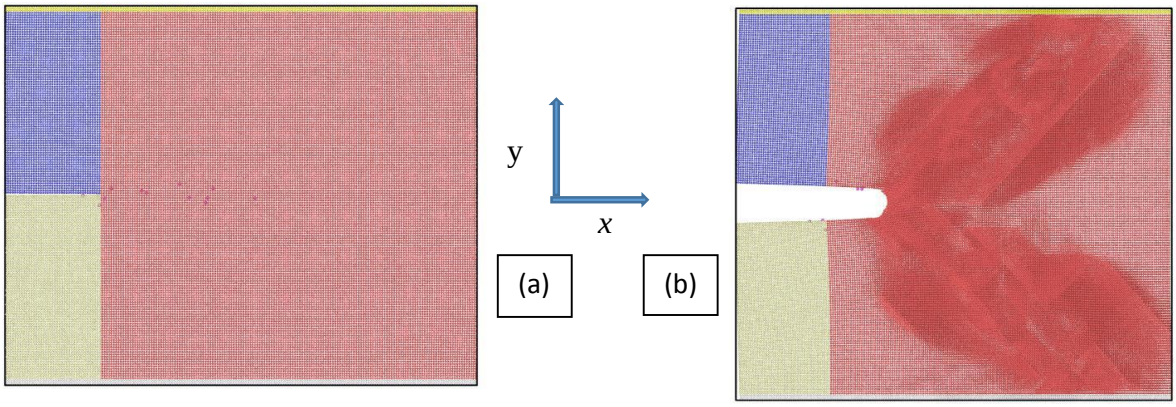


*Figure 25. 'Double-Single' with 0.1% hydrogen (a) Crack at T=0 ps, (b) Crack at T=12 ps*

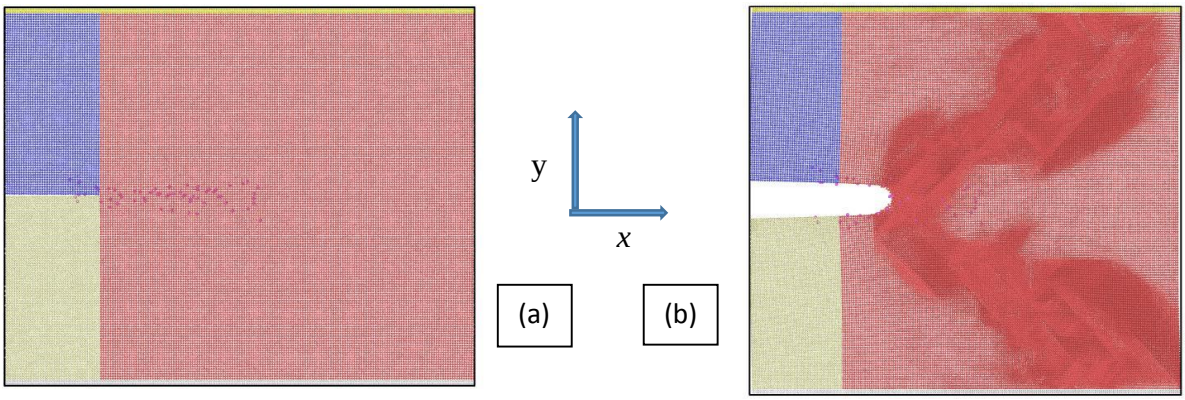


*Figure 26. 'Double-Single' with 0.5% hydrogen (a) Crack at T=0 ps, (b) Crack at T=12 ps*

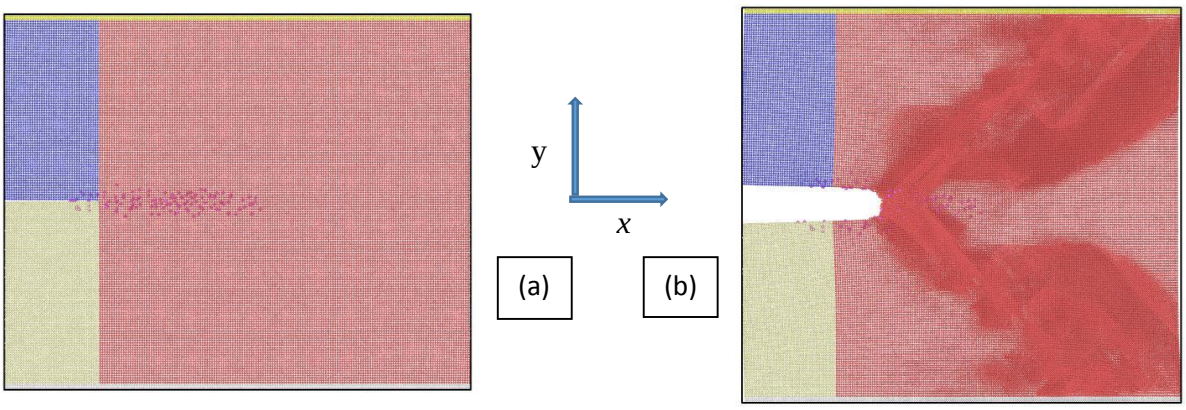


*Figure 27. 'Double-Single' with 1% hydrogen (a) Crack at T=0 ps, (b) Crack at T=12 ps*

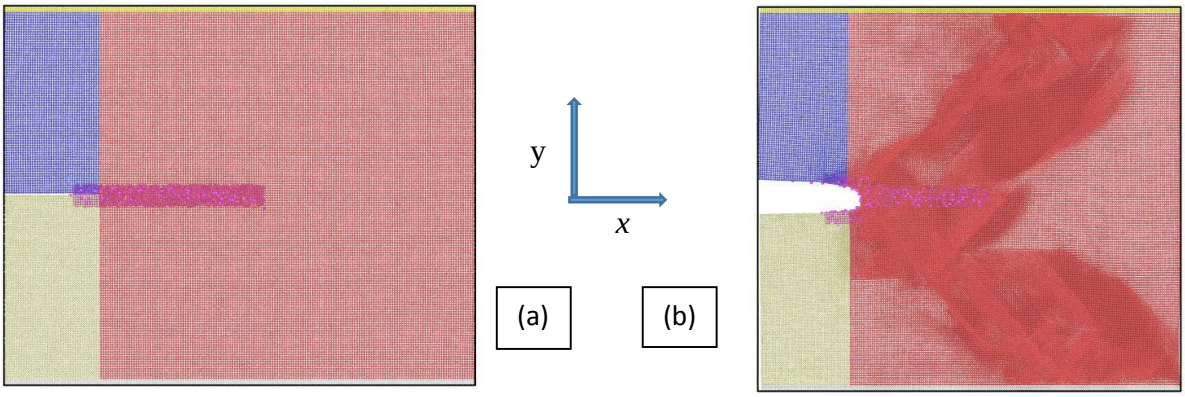


*Figure 28. 'Double-Single' with 10% hydrogen (a) Crack at T=0 ps, (b) Crack at T=12 ps*

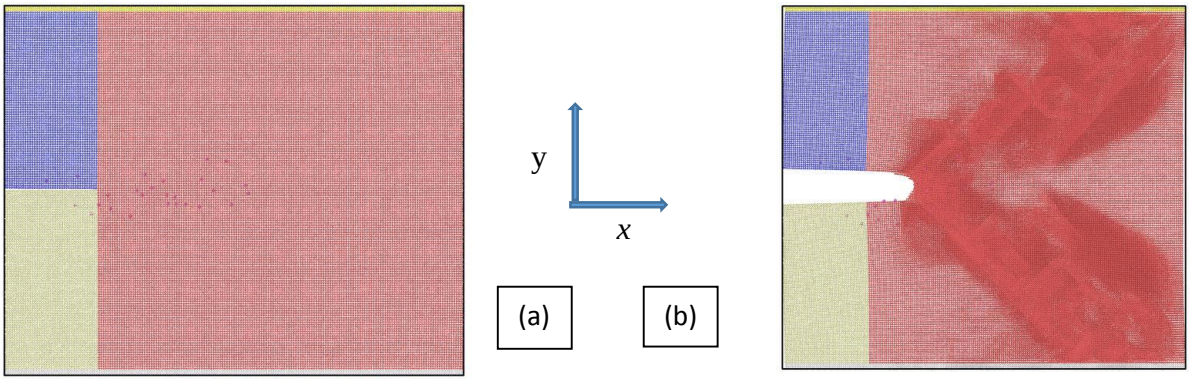


*Figure 29. 'Double-Double' with 0.1% hydrogen (a) Crack at T=0 ps, (b) Crack at T=12 ps*

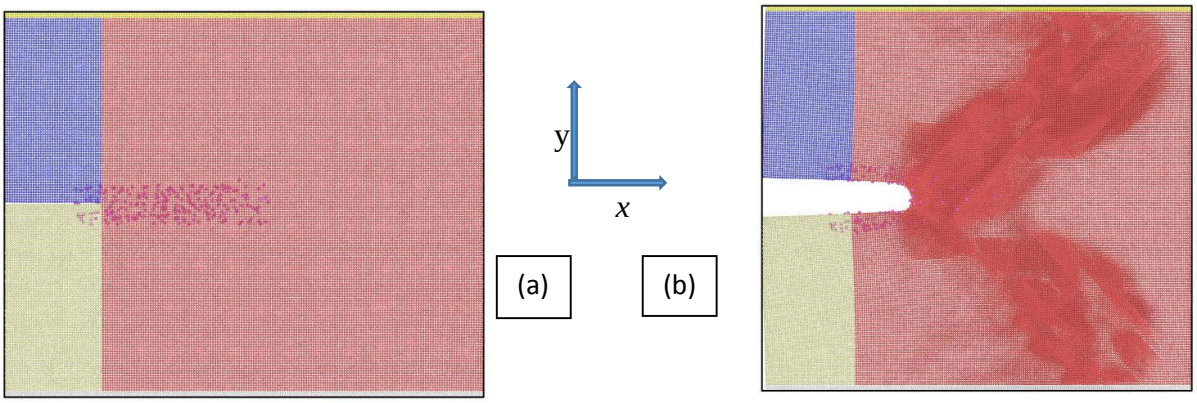


*Figure 30. 'Double-Double' with 0.5% hydrogen (a) Crack at T=0 ps, (b) Crack at T=12 ps*

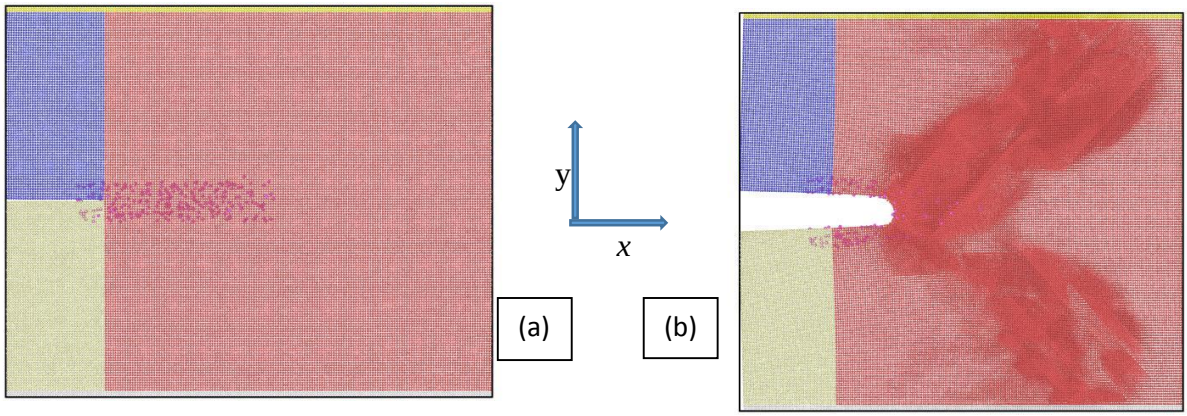


*Figure 31. 'Double-Double' with 1% hydrogen (a) Crack at T=0 ps, (b) Crack at T=12 ps*

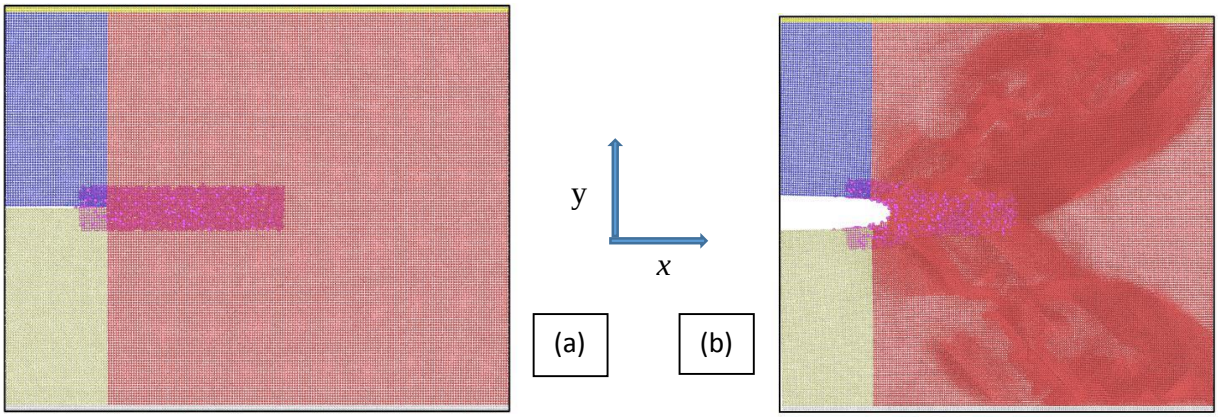


*Figure 32. 'Double-Double' with 10% hydrogen (a) Crack at T=0 ps, (b) Crack at T=12 ps*